This is a brief description of the methods used in the code for atomic structure calculations (for single-valence systems), and has definitions for all the relevant equations. The code is available online: github.com/benroberts999/ampsci; see the "readme" file for compiling/usage instructions. Some basic documentation for the code is also available: benroberts999.github.io/ampsci/. This is not meant as a complete description of the physics, but references are provided to more detailed descriptions.

1 Radial Dirac equation (spherical potentials)

Using atomic units[1], the single-electron Dirac equation is

$$(H_D - \varepsilon)\,\phi(\boldsymbol{r}) = 0, \tag{1}$$

where H_D is the Dirac Hamiltonian (see, e.g., [1]):

$$H_D = c\boldsymbol{\alpha}\cdot\boldsymbol{p} + c^2(\beta - 1) + \hat{V}, \tag{2}$$

and $\boldsymbol{\alpha} = \gamma^0\boldsymbol{\gamma}$ and $\beta = \gamma^0$ are Dirac matrices. Note that we have subtracted the electron rest energy, so the total relativistic energy is $E = \varepsilon + c^2$ (for positive total energy states). For bound states, $\phi \to 0$ as $r \to \infty$ and ϕ is regular everywhere and thus normalisable. The set of solutions $\{\phi_i\}$ (including the negative energy states) to (1) form a complete orthogonal set/basis. We use the standard normalisation choice, so that $\langle\phi_i|\phi_j\rangle = \delta_{ij}$. Wavefunctions for many-electron atoms are formed from single-particle orbitals, see, e.g., Ref. [2].

For spherically symmetric potentials $\hat{V}$, we can express the four-component single-particle orbitals in the form[2,3]:

$$\phi_{n\kappa m}(\boldsymbol{r}) = \frac{1}{r}\begin{pmatrix} f_{n\kappa}(r)\,\Omega_{\kappa m}(\boldsymbol{n}) \\ i g_{n\kappa}(r)\,\Omega_{-\kappa,m}(\boldsymbol{n}) \end{pmatrix}, \tag{3}$$

where $\kappa = (l-j)(2j+1)$ is the Dirac quantum number, and Ω is a (two-component) spherical spinor,

$$\Omega_{\kappa m} \equiv \sum_{s_z=\pm1/2} \langle l, m-s_z, 1/2, s_z|j,m\rangle\, Y_{l,m-s_z}(\boldsymbol{n})\,\chi_{s_z}, \tag{4}$$

with $\langle j_1 m_1 j_2 m_2|JM\rangle$ a Clebsch-Gordon coefficient, Y_{lm} a spherical harmonic, $\boldsymbol{n} = \boldsymbol{r}/r$, and χ_{s_z} is a spin eigenstate [$\chi_{1/2} = (1,0)^T$, $\chi_{-1/2} = (0,1)^T$]. The terms in ϕ are orthonormal as:

$$(n\kappa|n'\kappa) \equiv \int (f_{n\kappa}f_{n'\kappa} + g_{n\kappa}g_{n'\kappa})\,\mathrm{d}r = \delta_{n'n} \tag{5}$$

$$\langle\kappa m|\kappa' m'\rangle \equiv \int \left(\Omega^\dagger_{\kappa m}\Omega_{\kappa' m'}\right)\mathrm{d}\Omega = \delta_{\kappa'\kappa}\delta_{m'm}. \tag{6}$$

Then, we can define the radial Dirac equation in the form:

$$(H_r - \varepsilon)\,F_{n\kappa} = 0, \tag{7}$$

where we defined the *radial spinor*,[4]

$$F_{n\kappa} = \begin{pmatrix} f_{n\kappa}(r) \\ g_{n\kappa}(r) \end{pmatrix}, \tag{8}$$

and *radial Hamiltonian*,

$$H_r = \begin{pmatrix} \hat{V} & c(\frac{\kappa}{r} - \partial_r) \\ c(\frac{\kappa}{r} + \partial_r) & \hat{V} - 2c^2 \end{pmatrix}. \tag{9}$$

The 3D (spherical) Hamiltonian can also be expressed in this form by replacing κ in (9) with $-\hat{k}$ (top right) and $\hat{k}$ (bottom left), where $\hat{k} \equiv -1 - \boldsymbol{\sigma}\cdot\boldsymbol{l}$, and $\hat{k}\Omega_{\kappa m} = \kappa\Omega_{\kappa m}$. I will suppress the r subscript and use $(H-\varepsilon)\,F = 0$ and $(H-\varepsilon)\,\phi = 0$ interchangeably, since there is no risk of confusion.

1.1 Nuclear and electron potentials[5]

For a many-electron atom, the potential term consists of the sum of the nuclear and inter-electron potentials:

$$\hat{V} = V_{\text{nuc}} + V_{\text{el}}. \tag{10}$$

The electron potential involves a large number of complicated terms and must be taken into account approximately (as discussed in the following sections). For a point-like nucleus, $V_{\text{nuc}} = -Z/r$; in reality, the nuclear charge is distributed across the finite-size nucleus. To form V_{nuc}, we assume the nuclear charge is distributed according to a Fermi distribution,

$$\rho(r) = \rho_0\,(1 + \exp[(r-c)/a])^{-1}, \tag{11}$$

where ρ_0 is the normalisation factor, ($\int \rho\,\mathrm{d}V = Z$), c is the half-density radius, and a is defined via the 90–10% density fall-off $t \equiv 4a\ln 3$ (known as the "skin thickness"), which we take to be $t = 2.3\,\text{fm}$ for all heavy isotopes. The half-density radius is related to a and r_{rms}, the root-mean-square charge radius, as $c = \sqrt{(5r^2_{\text{rms}} - 7\pi^2a^2)/3}$. Then, V_{nuc} is obtained numerically from (11) using Gauss' law. The code also allows you to assume a spherical nucleus (mainly used for testing).

2 Numerical solution to the Dirac equation[6]

2.1 Bound-state solution to local Dirac equation

From Eq. (7), we can express the radial derivative as:

$$\partial_r F = \frac{1}{c}\begin{pmatrix} -c\,\kappa/r & (\varepsilon - \hat{V} + 2c^2) \\ -(\varepsilon - \hat{V}) & c\,\kappa/r \end{pmatrix} F, \tag{12}$$

which has the familiar form of an ODE. Very roughly, we can solve an ODE numerically by stepping forward if we know the derivative of a function, and the value of the function at some previous point:

$$F(r+\delta r) \approx F(r) + \frac{\partial F(r+\delta r)}{\partial r}\delta r. \tag{13}$$

This can be re-written as

$$F(r) \approx [1 - D(r+\delta r)\delta r]\,F(r+\delta r),$$

were D is the derivative operator, which can be written, for a specific position r, as a 2x2 matrix according to Eq. (12). Therefore, we can solve for $F(r+\delta r)$ algebraically:

$$F(r+\delta r) \approx [1 - D(r+\delta r)\delta r]^{-1}\,F(r).$$

[1] $\hbar = m_e = e = |e| = 1$, $c = 1/\alpha \approx 137$

[2] We use the Dirac basis; see Appendix A.4.

[3] Our notation differs from some other places: compared to Ref. [1] we have $f \leftrightarrow g$; compared to [3] we have $f_{\text{here}} = P_{\text{Johnson}}$, $g_{\text{here}} = -Q_{\text{Johnson}}$; compared to Ref. [4] we have $g_{\text{here}} = \alpha g_{\text{Dzuba}}$; and compared to Ref. [5] we have $f_{\text{here}} = g_{\text{Sapirstein}}$ and $g_{\text{here}} = -f_{\text{Sapirstein}}$.

[4] Radial spinor defined in: /src/Wavefunction/DiracSpinor.hpp

[5] Nuclear potentials defined in: /src/Physics/NuclearPotentials.hpp

[6] Functions to solve Dirac equation defined in: /src/DiracODE/

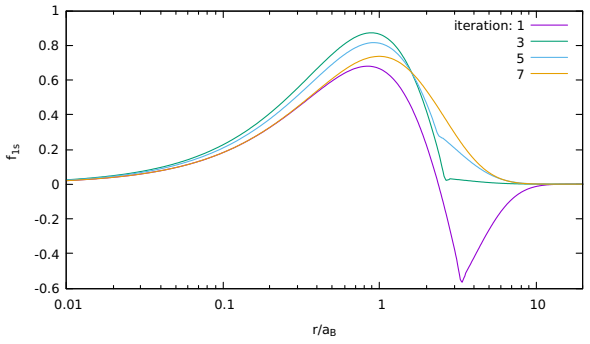

Figure 1: Hydrogen 1s orbital, as calculated at the first though 7th iteration. For this example, the initial energy guess was -0.3au, and converged to $-0.500006566..$ to parts in 10^{-16} in 12 iterations.

As written, this method is far too crude, owing to the very rough approximation used in Eq. (13). More accurate approaches, known as multi-step methods, approximate the value of the derivative along the interval $(r,\, r+\delta r)$ with greater accuracy by using more previous points in the estimation. The specific method we use (Adams-Moulton method) is described in detail in Ref. [3].

In general, Eq. (12) will have solutions for any given ε. We are typically interested in the specific bound-state solutions, for which $F \to 0$ as $r \to \infty$, and $F(0) = 0$. To solve the bound-state problem, an initial ε is guessed, and the DE is solved using the multi-step method. Then, small adjustments are made to ε until (a) we have the correct state $(n\kappa)$ determined by the number of nodes of the orbital $(n-l-1)$, and (b) we have the correct boundary conditions.

In order to use the multi-step method, a few initial points of the radial F function are required. These are determined by solving the asymptotic form of the Dirac equation analytically accounting for the boundary conditions. It is common to expand the orbital around $r = 0$ to start the procedure, and then adjust the energy until $F \to 0$ at infinity. A more numerically stable approach, however, is to solve the DE twice, once starting from $r = 0$, and once from $r = \infty$ [3]. These two solutions are stepped inwards toward some central point, where the two solutions are joined – one of the two solutions is re-scaled so that $f_0 = f_\infty$ at the defined point. Small energy adjustments are made until the lower g components also match at this point (this ensures the derivatives match, and the join is smooth). In our case, the two solutions are not joined at a single point, but are instead "meshed" across a few (~ 10) points around the classical turning point, defined via $V(r_{\rm ctp}) = \varepsilon$. The meshing procedure acts to smooth out numerical noise, and makes the method more numerically stable. This procedure typically allows convergence of the energies to parts in 10^{16}; see Fig. 1 for an example.

Note that Eq. (12) does not determine the normalisation for F, so the solutions must be normalised explicitly [Eq. (5)]. Further, the sign of F is also arbitrary from Eq. (12); we choose $f(r)$ to be positive as $r \to 0$, as is standard.

Everywhere in the code, the fine structure constant is replaced with: $\alpha \to \lambda\alpha_0$ (in atomic units, $\alpha = 1/c$), where $\alpha_0 \approx 1/137$. The factor λ is a run-time input option, that is 1 by default. For example, letting $\lambda \to 0$ (i.e., $c \to \infty$) allows us to perform calculations in the non-relativistic limit. This is a particularly useful option for checking the calculations, and for determining the sensitivity of particular observables to variations in the fine structure constant. Modifications can also be made to the above equations to account for the finite electron/nucleus mass (reduced mass) – but this is not implemented in the code.

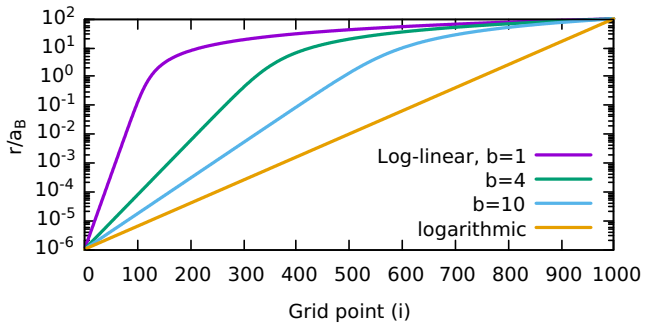

Figure 2: Radial distance r_i as function of grid-point, i.

2.2 Radial grid[7]

The equations are solved numerically on a finite radial grid (the orbitals are stored in arrays on this grid). We define a grid on the region from r_0 to $r_{\rm max}$, that has N points.

We don't use a uniformly spaced grid, since the wavefunctions vary very rapidly at small distances, but rather slowly at large distances. We define a non-uniformly-spaced radial grid (r_i) in terms of a uniformly spaced u grid $(u_{i+1} = u_i + \delta u)$. In this case, integrals become:

$$\int_0^\infty f(r)\,\mathrm{d}r \to \int_{r_0}^{r_{\rm max}} f(r)\,\mathrm{d}r \to \int_{u_0}^{u_{\rm max}} f(r(u))\frac{\mathrm{d}r}{\mathrm{d}u}\,\mathrm{d}u, \qquad (14)$$

which numerically becomes:

$$\int_{u_0}^{u_{\rm max}} f(r(u))\frac{\mathrm{d}r}{\mathrm{d}u}\,\mathrm{d}u \to \sum_{i=0}^{N-1} f(r_i)\frac{\mathrm{d}r}{\mathrm{d}u}\Big|_i \delta u \qquad (15)$$

(in the code we actually use a quadrature integration formula for the integrals). The initial/final grid points and the grid spacings must be chosen such that the above numerical approximations are sufficiently accurate.

In the code, we can set either a logarithmic grid, defined:

$$u = \ln(r), \qquad \frac{\mathrm{d}r}{\mathrm{d}u} = r, \qquad (16)$$

or a mixed log-linear grid, defined:

$$u = r + b\ln(r), \qquad \frac{\mathrm{d}r}{\mathrm{d}u} = \frac{r}{r+b}, \qquad (17)$$

which is approximately logarithmic at small distances $(r < b)$, and approximately linear at large distances (typically $b \sim 10\,a_0$); see Fig. 2. The logarithmic grid works very well, and allows good convergence without requiring a large number of points, but works less well for highly excited states, and works quite poorly for continuum states with high energy. The log-linear grid works well in a wide range of cases, but often needs more grid points to achieve the same numerically accuracy[8].

2.3 Dirac equation involving inhomogeneous or non-local terms (Green's Method)

This is a brief overview only; for explanations/proofs see, e.g., Ref. [6]. Consider the inhomogeneous Dirac equation, with extra

[7] Radial grid defined in: /src/Maths/Grid.hpp

[8] The code also allows the use of linear grid – but this requires a very large number of points to work, so should only be used for testing.

'source' term S:

$$(H_\mathrm{l} - \varepsilon)\, F = S, \tag{18}$$

where H_l is a Dirac Hamiltonian involving only local potential terms. We solve this for a normalisable F using the Green's method for ODEs. First, take the homogeneous equation:

$$(H_\mathrm{l} - \varepsilon)\, G = 0, \tag{19}$$

which we solve (for a given energy ε) using the regular linear ODE multi-step methods from Sec. 2.1. Note that since F is a normalisable solution to (18) G will *not* (in general) be a normalisable solution to (19) [i.e., G is not regular at the origin/infinity]. Instead, we seek two solutions, which are each bound by one of the boundary conditions; i.e., one solution that satisfies the boundary condition at the origin, G_0, and a second that satisfies that at infinity, G_∞. Then, the normalisable solution to (18) that satisfies both boundary conditions is:

$$F(r) = G_\infty(r) \int_0^r \frac{G_0(r')^T\, S(r')}{c\, w(r')}\, \mathrm{d}r' + G_0(r) \int_r^\infty \frac{G_\infty(r')^T\, S(r')}{c\, w(r')}\, \mathrm{d}r' \tag{20}$$

$(A^T B \equiv f_A f_B + g_A g_B)$ where $c = 1/\alpha$. The Wronskian,

$$w(r) = f_\infty(r) g_0(r) - f_0(r) g_\infty(r), \tag{21}$$

should be independent of r.

Note that this method clearly doesn't work if $w = 0$; worse, the method can be numerically unstable if S and w are both small (if S is too small, it implies the $G_{0,\infty}$ solutions will be similar, and thus w will be small).

2.4 Continuum orbitals

We are sometimes interested in continuum orbitals that are regular at the origin (see, e.g., Ref. [1]). For continuum orbitals of the desired energy $\varepsilon > 0$, we solve using the multi-step method described above, starting from the origin and integrating outwards. Note that we do not have $F_c \to 0$ at large r, and continuum orbitals cannot be normalised as above. For most problems, however, we do require normalised orbitals.

We choose energy normalisation [1]:

$$\int_{\varepsilon-\delta\varepsilon}^{\varepsilon+\delta\varepsilon} \langle \varepsilon' \kappa m | \varepsilon \kappa m \rangle\, \mathrm{d}\varepsilon' = 1. \tag{22}$$

This equation cannot be used directly. Instead, the orbitals are normalised in analogy with analytic Coulomb (H-like) continuum states. For Coulomb potentials, at large r we have:

$$f(r) \approx \sqrt{\frac{\alpha}{\pi\beta}}\, \sin(kr + \ldots), \tag{23}$$

with $\beta = \sqrt{\varepsilon/(\varepsilon + 2c^2)}$ (other terms in sine function are either constant, or logarithmic in r). At large r, the atomic potential is also Coulomb-like. We use (23) to normalise the orbitals by enforcing the amplitude of the sine-like orbitals at large r to match the analytic H-like solutions [1].

To do this, we have to extend the radial grid out to very large distances, often much larger than the normal grid used to solve the bound-state orbitals. The orbital is solved out to large r until the amplitude/frequency of the oscillations becomes close enough to constant, and then the amplitude is re-scaled to match (23). After solving, the orbital is only kept up until r_max, since larger distances typically do not contribute to any required radial integrals.

3 Hartree-Fock (self-consistent field method)[9]

The many-body atomic Hamiltonian may be expressed as

$$H = \sum_i h_0(\boldsymbol{r}_i) + \sum_{i<j} \frac{1}{|\boldsymbol{r}_i - \boldsymbol{r}_j|}, \tag{24}$$

where

$$h_0 = c\boldsymbol{\alpha}\cdot\boldsymbol{p} + c^2(\beta - 1) + \hat{V}_\mathrm{nuc},$$

is the single-particle Dirac Hamiltonian including only the nuclear potential. In order to solve the single-particle Dirac equation for an N electron atom, we replace the complicated electron-electron repulsion term with an approximate potential:

$$H \approx \sum_i h_0(\boldsymbol{r}_i) + \sum_i V_{\mathrm{avg,i}}(\boldsymbol{r}_i), \tag{25}$$

where V_avg is the average potential due to the other $(N-1)$ electrons. For a given V_avg, this equation yields a complete set of orthogonal single-particle orbitals; many-body wavefunctions can be expressed Slater-determinants formed from these orbitals, see, e.g., [2, 3]. This section concerns calculating V_avg.

For any general "self-consistent field method", we start with an initial approximation for the electronic potential (e.g., Thomas-Fermi potential, or a simple parametric potential), and use this to generate a set of orbitals for the desired subset of atomic electrons (e.g., the core). The total electron density formed from these orbital tells us the electronic charge distribution across the atom, which we use to generate a new electronic potential (Gauss' law). In general, this new potential will be a better approximation for the true electronic potential than the initial guess. A new set of orbitals formed in this better potential will be a better set of orbitals, which we use to generate a better-yet potential and so on, until convergence is reached. At the end, the potential used to form the electron orbitals should be the same as the potential that is formed from the electron orbitals, and is thus self-consistent.

3.1 Relativistic Hartree-Fock method

The method we use to find the self-consistent potential is the relativistic Hartree-Fock method, which includes the electron exchange interaction. This section largely follows the detailed explanation from Ref. [3], with a few extensions. In the Hartree Fock approximation, the single-particle Dirac equation is

$$(H_\mathrm{HF} - \varepsilon)\, \phi(\boldsymbol{r}) = 0, \tag{26}$$

with the Hartree Fock Hamiltonian,

$$H_\mathrm{HF} = c\boldsymbol{\alpha}\cdot\boldsymbol{p} + c^2(\beta - 1) + \hat{V}_\mathrm{HF}. \tag{27}$$

Here, $\hat{V}_\mathrm{HF}$ is the Hartree Fock potential. We consider mainly atoms with a single valence electron above closed shells, and take the Hartree-Fock potential to be the potential due to the $N-1$ core electrons. This is called the $V^{(N-1)}$ potential.

By minimising the many-body energy for the single Slater-determinant electronic wavefunction (see textbook [3] for details), the Hartree-Fock potential can be derived as

$$\hat{V}_\mathrm{HF}\phi_a(\boldsymbol{r}_1) = \sum_{i\neq a}^{N_c} \left(\int \frac{\phi_i^\dagger(\boldsymbol{r}_2)\phi_i(\boldsymbol{r}_2)}{|\boldsymbol{r}_{12}|} \mathrm{d}^3\boldsymbol{r}_2\, \phi_a(\boldsymbol{r}_1) - \int \frac{\phi_i^\dagger(\boldsymbol{r}_2)\phi_a(\boldsymbol{r}_2)}{|\boldsymbol{r}_{12}|} \mathrm{d}^3\boldsymbol{r}_2\, \phi_i(\boldsymbol{r}_1) \right), \tag{28}$$

[9] Method implemented in: /src/HF/HartreeFock.hpp

where the sum over i extends over all occupied electrons $i = \{n_i, \kappa_i, m_i\}$. The Coulomb integrals are computed by expanding r_{12}^{-1} in terms of spherical harmonics (Laplace expansion) – see Appendix A.2. Integrating over angles, and summing over m quantum numbers we have:

$$\hat{V}_{\rm HF}F_a(r) = \left(\sum_b [j_b]x_b\, y^0_{bb}(r)\right) F_a(r) - \frac{1}{[j_a]}\sum_b \tilde{x}^a_b \sum_k (C^k_{ab})^2\, y^k_{ab}(r)F_b(r) \quad (29)$$

$$\equiv V_{\rm dir}(r)\, F_a(r) + [\hat{V}_{\rm ex}F_a](r), \quad (30)$$

where now the b sum extends over all occupied *orbitals* (i.e., $b = \{n_b, \kappa_b\}$), y^k_{ab} is a symmetric Coulomb integral (sometimes called Hartree screening functions, or Hartree Y functions),

$$y^k_{ab}(r) = \int_0^\infty \frac{r^k_<}{r^{k+1}_>}\left[f_a f_b + g_a g_b\right](r')\,{\rm d}r', \quad (31)$$

with $r_< = \min(r, r')$, and C^k_{ab} is the angular factor,

$$C^k_{ab} \equiv \langle\kappa_a||C^k||\kappa_b\rangle = (-1)^{j_a+1/2}\sqrt{[j_a][j_b]}\times \begin{pmatrix} j_a & j_b & k \\ -1/2 & 1/2 & 0\end{pmatrix}\pi(l_a + l_b + k). \quad (32)$$

Here, $\pi(x) = 1(0)$ if x is even(odd), and $[x] \equiv 2x + 1$. The x_b term is the occupation fraction for shell b, and $\tilde{x}^a_b = x_b$ when $b \neq a$, but $\tilde{x}^a_a = 1$ ($x_b = 1$ for closed shell; this is an approximate way for treating HF equations for open-shell systems[10]).

The Hartree-Fock method is the ideal starting point for many-body calculations, since all first-order corrections to the HF potential (i.e., corrections involving single core excitations) cancel exactly [2]. Corrections to energies and wavefunctions only arise at the second-order of perturbation theory.

Hartree-Fock algorithm:

- Form initial set of core orbital using guess for $V_{\rm el}(r)$[11]
- Begin HF routine:
  - Form new $V_{\rm dir}$, Eq. (29)
  - For each orbital
    - Form new $V_{\rm exch}\phi$, Eq. (29)
    - Solve inhomogeneous Dirac Equation (Sec. 3.2)
    - Adjust energy until ϕ is eigenstate (Sec. 3.3)
  - Continue HF routine until $\Delta\varepsilon/\varepsilon < \epsilon_{\rm cut}$ for all states
- HF (core) has converged. "Freeze" $V_{\rm dir}$ and orbitals $\{\phi_c\}$
- Do HF for each valence state (from "For each orbital")

In the code, we perform the HF procedure for the core twice, first using an approximate localised form of the exchange potential $V_{\rm exch}$. This extra step is not necessary, and is only done to speed up the convergence (it provides more realistic orbitals as a starting point for the non-local HF equations). The approximate potential will be shown in Sec. 3.4. Plots of the electron density ($\rho = \sum_n |\psi_n|^2$) for Cs are shown in Fig. 3, as calculated in varying approximations.

[10] The i sum in (28) includes a sum over all occupied m states; for partially filled shells, this doesn't include all m values. So, to do the sum, we assume each m is filled with equal probability – i.e., that each m is partially filled. We assume non-relativistic filling (e.g., $p_{1/2}$ and $p_{3/2}$ on equal footing).

[11] Essentially any approximation will do, so long as the combined nuclear and electronic potentials have $V(r \to 0) \approx -Z/r$, and $V(r \to 0) \approx -\xi/r$, where $\xi = 1$ for a neutral atom. I use a simple parametric potential [7].

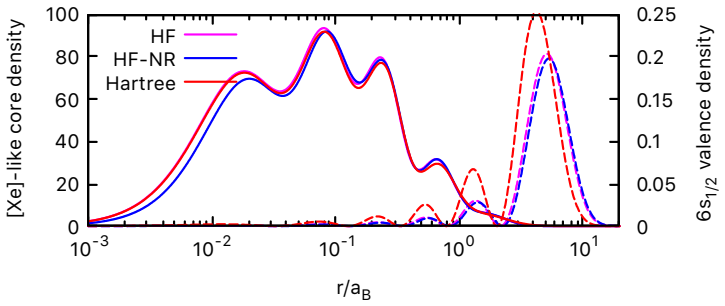

Figure 3: Electron density $\rho = \sum_n |\psi_n|^2$ for the core (solid line) and $6s$ valence (dashed line) electrons for Cs in the relativistic Hartree-Fock (HF), non-relativistic Hartree Fock (HF-NR), and Hartree approximations. Relativistic effects "pull" the electrons closer to the nucleus, and the exchange interaction is crucial for valence states.

The HF procedure converges to the level of $\epsilon \simeq 10^{-13}$. The resulting core orbitals are correct eigenstates (that is, the energy calculated in the HF routine is the same as $\langle\phi|H|\phi\rangle$) to the level of $\sim 10^{-11}$; see Table 1. The HF orbitals are also correctly orthogonal to better than $\sim 10^{-6}$; e.g., for Cs, the orthogonality for the worst core-core and valence-valence states are calculated: $\langle 5s_{1/2}|2s_{1/2}\rangle \simeq 2\times10^{-6}$ and $\langle 7s_{1/2}|6s_{1/2}\rangle \simeq 1\times10^{-7}$.

3.2 Solving the HF equation for given orbital

To solve the HF equation for a given orbital, we use the Green's method as outlined above. The HF Hamiltonian is split in to local and non-local parts as $H_{\rm HF} = H_{\rm l} + V_{\rm nl}$, with

$$H_{\rm l} = H_0 + V_{\rm nuc} + fV_{\rm dir}, \quad (33)$$

$$V_{\rm nl} = (1-f)V_{\rm dir} + V_{\rm exch}. \quad (34)$$

Here,

$$f = \begin{cases} (N_c - 1)/N_c & \text{core} \\ 1 & \text{valence}\end{cases} \quad (35)$$

is chosen so that $V_{\rm l} = V_{\rm nuc} + fV_{\rm dir} \to -Z_{\rm ion}/r$ as $r \to \infty$ (otherwise, we would have $V_{\rm l} \to 0$). This is done to ensure the existence of the solution that is regular at infinity (G_∞), and so that the asymptotic behaviour of the homogeneous solutions (19) match that of the final solution.

Then, the inhomogeneous equation has the form of Eq. (18):

$$(H_{\rm l} - \varepsilon)\, F = -V_{\rm nl}F. \quad (36)$$

Note that the "source" term in this case contains the solution F. So the equations must be solved iteratively, with some starting approximation for the source term, so that the solution at the nth step depends on the approximate solution from the previous step. Further, $V_{\rm nl}$ and $H_{\rm l}$ also depend on the solution F via (30), and these are also formed at the nth step using $F^{(n-1)}$. That is, the equation we solve at each iteration is

$$\left(H_0 + V_{\rm nuc} + fV^{(n-1)}_{\rm dir} - \varepsilon\right)F^{(n)} = -\left((1-f)V^{(n-1)}_{\rm dir} + V^{(n-1)}_{\rm exch}\right)F^{(n-1)}. \quad (37)$$

The energy guess used for the $(n+1)$th step can be approximated as $\varepsilon^{(n)} + \delta\varepsilon$, with

$$\delta\varepsilon \approx \frac{\langle F^{(n-1)}|\Delta V|F^{(n)}\rangle}{\langle F^{(n-1)}|F^{(n)}\rangle} \quad (38)$$

Table 1: Comparison of Hartree-Fock energies with expectation value of Hamiltonian for Cs (test of numerical accuracy).

ψ	$\langle\psi\|H\|\psi\rangle$	$\varepsilon_{\rm HF}$	ϵ^*	ψ	$\langle\psi\|H\|\psi\rangle$	$\varepsilon_{\rm HF}$	ϵ
$1s$	−1330.11874784318	−1330.11874784821	-4E-12	$4d_{3/2}$	−3.48561893015	−3.48561893030	-4E-11
$2s$	−212.56445398158	−212.56445398576	-2E-11	$4d_{5/2}$	−3.39690162346	−3.39690162364	-5E-11
$2p_{1/2}$	−199.42945475153	−199.42945475392	-1E-11	$5s$	−1.48980540326	−1.48980540357	-2E-10
$2p_{3/2}$	−186.43656610582	−186.43656610730	-8E-12	$5p_{1/2}$	−0.90789795941	−0.90789795957	-2E-10
$3s$	−45.96974036708	−45.96974036910	-4E-11	$5p_{3/2}$	−0.84033954719	−0.84033954740	-3E-10
$3p_{1/2}$	−40.44829871452	−40.44829871568	-3E-11	Valence states:			
$3p_{3/2}$	−37.89430454749	−37.89430454870	-3E-11	$6s$	−0.12736806899	−0.12736806898	7E-11
$3d_{3/2}$	−28.30950025207	−28.30950025207	-1E-14	$7s$	−0.05518735931	−0.05518735931	4E-11
$3d_{5/2}$	−27.77515677536	−27.77515677489	2E-11	$6p_{1/2}$	−0.08561588462	−0.08561588462	-5E-11
$4s$	−9.51282144793	−9.51282144936	-1E-10	$7p_{1/2}$	−0.04202138669	−0.04202138668	2E-10
$4p_{1/2}$	−7.44628469483	−7.44628469556	-1E-10	$6p_{3/2}$	−0.08378548243	−0.08378548242	1E-10
$4p_{3/2}$	−6.92100118797	−6.92100118878	-1E-10	$7p_{3/2}$	−0.04136804383	−0.04136804383	5E-11

$^*\epsilon \equiv (\langle\psi|H|\psi\rangle - \varepsilon_{\rm HF})/\varepsilon_{\rm HF}$

where $\Delta V = V_{\rm HF}^{(n)} - V_{\rm HF}^{(n-1)}$. Instead of storing $F^{(n-1)}$ and $V_{\rm HF}^{(n-1)}$ for each iteration, we use $F^{(0)}$ and calculate the energy guess with respect to $\varepsilon^{(0)}$.

In general, these solutions will not be correct eigenstates of the HF Hamiltonian and won't be correctly normalised. We therefore make small adjustments to the energy and orbital until F is properly normalised and thus an eigenstate of the Hamiltonian. This procedure is outlined in the next subsection 3.3.

Once the energy has been fine-tuned, and we have a normalised eigenstate, we continue the HF procedure. To aid convergence, however, we first "damp" the orbitals as:

$$F \to (1-\eta)F + \eta F_{\rm old}. \tag{39}$$

This both increases the numerical stability, and speeds up the convergence. Typically, $\eta \sim 0.5$; in the code, η is initially set to a large value (0.8), and is slowly ramped down (to 0.1) over the HF iterations (0 means no damping). So long as the equations converge, the solutions do not depend on the value chosen.

3.3 Energy adjustments – finding eigenstate

Assume the correct orbital and energy can be written as $F+\delta F$, and $\varepsilon+\delta\varepsilon$, where F was the solution to Eq. (37) using the trial energy ε. Subbing this back into the HF Dirac equation, we find a new inhomogenous equation (to first order):

$$(H_{\rm HF} - \varepsilon)\delta F = \delta\varepsilon F \tag{40}$$
$$(H_{\rm l} - \varepsilon)\delta F = \delta\varepsilon F - V_{\rm nl}\delta F, \tag{41}$$

which we solve iteratively for δF and $\delta\varepsilon$. As the first step, we divide (41) by the unknown $\delta\varepsilon$, set $V_{\rm nl}\delta F = 0$, and solve for $\tilde{F} \equiv \delta F/\delta\varepsilon$ using Green's method (20). Note that we don't need to re-solve the homogeneous equation (19), since we can re-use the G_∞, G_0 solutions obtained when solving (37).

Since $(F+\delta F)$ must be normalised, we find the first guess for $\delta\varepsilon$ as (keeping only first-order terms):

$$\delta\varepsilon = \frac{\langle F|F\rangle - 1}{2\langle F|\tilde{F}\rangle}. \tag{42}$$

Using $\delta F = \delta\varepsilon\tilde{F}$, we form $V_{\rm nl}\delta F$ and solve (41) for δF. Then, we make the corrections to the orbital and energy:

$$F \to F + \delta F\,, \qquad \varepsilon \to \varepsilon + \delta\varepsilon. \tag{43}$$

This iterative procedure is continued from Eq. (41) until the energy correction drops below a specified value (i.e., until F is properly normalised). This procedure is very rapid; e.g., $\delta\varepsilon/\varepsilon$ typically converges to parts in 10^{20} with just two iterations.

Note that, so long as it was chosen appropriately, the non-local term $V_{\rm nl}$ is small, and so the $V_{\rm nl}\delta F$ term is even smaller and can be excluded entirely in this section without having much of an impact. Including it, however, leads to better overall convergence of the HF equations. Note that $V_{\rm nl}\delta F$ includes $V_{\rm exch}\delta F$, which must be calculated.

3.4 Approximate "local" exchange potential

There are several methods for obtaining a localised approximation to the HF potential, a common example is the "Hartree-Fock-Slater" method [8]. Here, I outline a slightly different method that gives reasonably good results. We use this only as a starting point for the HF/TDHF procedures, so the the final result does not depend on this potential. The choice of a good starting approximation does, however, greatly speed up the convergence of the iterative procedures.

Introducing the notation v^x_{ab} [see Eq. (29)], the non-local exchange part of the HF potential can be expressed

$$[\hat{V}_{\rm ex}F_a](r) = \sum_b v^x_{ab}(r)F_b(r). \tag{44}$$

It is non-local in that it cannot be expressed as $\hat{V}_{\rm ex}(r)\,F_a(r)$. Multiply (44) from the right and divide by $F_a^\dagger F_a$:

$$\frac{[\hat{V}_{\rm ex}F_a]F_a^\dagger}{F_a^\dagger F_a}F_a = \frac{\sum_b v^x_{ab}(r)F_b(r)F_a^\dagger(r)}{F_a^\dagger F_a}F_a(r) \tag{45}$$
$$\approx U^{(a)}_{\rm ex}(r)F_a(r). \tag{46}$$

In this way we may define $U^{(a)}_{\rm ex}(r)$, which is a localised exchange potential (for state a). Note that $U(r)$ is different for each state, and depends on F_a, and therefore must be found iteratively.

In theory, this is exact except for when $F_a^\dagger F_a = 0$. In practice, it is very numerically unstable whenever $F_a^\dagger F_a$ is small. However, this is not a major problem, since when F_a is small, we don't care what the exchange potential is. We proceed by introducing a cut-off, λ_a, and only calculating the exchange potential when F_a is not small. Therefore, we write

$$U^{(a)}_{\rm ex}(r) = v^x_{aa}(r) + \sum_{b\neq a} v^x_{ab}(r)\Lambda(r) \tag{47}$$

with

$$\Lambda(r) = \begin{cases} \dfrac{F_a^\dagger(r)F_b(r)}{F_a^\dagger F_a} & |F_a(r)| > \lambda_a \\ 0 & \text{otherwise} \end{cases} \tag{48}$$

Of course, we don't apply the cut-off when $b = a$ in the sum, since here the cancellation is exact and there is no numerical instability. In fact, this $a = b$ term actually gives the dominating contribution to the exchange potential. Partly, the reason this method gives such good results already is that the dominating case is treated exactly.

In the code, the cut-off is taken as $\lambda_a = 10^{-2}|f_a|^{\max}$, where $|f|^{\max}$ is the maximum magnitude for the upper $f(r)$ component of F_a. Making the cut-off too small introduces numerical instabilities. This potential leads to very good approximations for the HF orbitals and energies, and as such leads to very quick convergence of both HF and TDHF equations. For example, with normal grid choices, the energies agree with complete HF energies to five digits, and the core orbitals are orthogonal to the level of $10^{-4} - 10^{-5}$.

4 Finite basis of orbitals[12]

In many problems in perturbation theory, a summation over the full (infinite) set of orbitals is required. In theory, a basis of HF orbitals can be used for this. However, such a basis generally converges very slowly, requires a very large radial grid, and the solutions become numerically unstable for low energies. Further, sum over all states must include the integral over all positive- and negative-energy continuum states, which can be a significant contribution. Instead, it is common to introduce a finite basis for the radial Dirac equation, see, e.g., Ref. [9]. We assert that all orbitals go to zero at the boundary of a subset of the radial grid, $r_{\max}$. This is equivalent to placing the atom in the centre of an infinite spherical "square-well" potential. In this case, a complete set of orbitals can be approximately expanded in terms of a finite number of states, which includes the $\varepsilon > 0$ continuum states. So long as the size of the cavity is large compared to typical radius of orbitals we are directly interested in, the results should be independent of the cavity size.

4.1 B-spline basis

The set of atomic orbitals are expanded as

$$F_{n\kappa} = \sum_i^{2N} p_i S_i(r), \tag{49}$$

where $\{S_i\}$ are a set of $2N$ basis orbitals that form a complete set over a sub-domain of the radial grid $[0, r_{\max}]$ (N is defined this way because of the duel set of positive/negative energy solutions to the Dirac equation). The $\{p_i\}$ expansion coefficients are found by diagonalising the set of basis orbitals with respect to the Hamiltonian matrix. In practise, this is done by solving the eigenvalue problem:

$$\langle S_i|\hat{H}_{\rm HF}|S_j\rangle p_i = \varepsilon \langle S_i|S_j\rangle p_i \tag{50}$$
$$H_{ij}p_i = \varepsilon S_{ij} p_i. \tag{51}$$

There are $2N$ solutions of eigenvalues ε with corresponding eigenvectors $\vec{p}$, which correspond to the spectrum of stationary states; N of these correspond to negative-energy ($\varepsilon < -mc^2$) states. If the S set is orthonormal, B is just the identity, but in general it is not. Note that A and B are positive-definite real matrices. States of different κ are orthogonal, so the A matrix can be chosen to be block diagonal (in κ); i.e. the expansion may be performed separately for each κ.

[12] Method implemented in: /src/Wavefunction/BSplineBasis.hpp

The choice of basis must account for the boundary conditions for the stationary states. A good choice of basis allows for convergence of many-body problems with fewer basis states. The particular choice we use is called the Duel-Kinetic-Balance (DKB) B-spline basis as introduced in Ref. [10];

$$S_i^{\rm DKB} = \begin{cases} \begin{pmatrix} b_i(r) \\ \frac{\alpha}{2}\left(\partial_r + \kappa/r\right) b_i(r) \end{pmatrix} & 0 \le i < N \\ \begin{pmatrix} \frac{\alpha}{2}\left(\partial_r - \kappa/r\right) b_{i-N}(r) \\ b_{i-N}(r) \end{pmatrix} & N \le i < 2N. \end{cases} \tag{52}$$

full details, including on including boundary conditions, are given in that work (see also [9, 11]). Note that the boundary conditions are met by discarding some of the underlying b-splines; when we talk of an expansion using N splines, we refer only to the ones that are kept; the underlying spline basis consists of a slightly larger set [10]. Another common choice, which we refer to as the Notre-Dame (ND) basis [9] may be formed with the lower-component of (52) set to zero for $i < N$, and the upper set to zero for $i \ge N$; this set requires extra conditions for the boundary conditions to be met [9].

Each B-spline, $b_i^{(k)}(r)$, is a polynomial of degree $k-1$, that is non-zero only in the interval $t_i \le r < t_{i+k}$, where $\{t_i\}$ are a set of $(N + k - 2)$ "knots" (the S_i basis orbitals are non-zero also only in this region). The first "interior" knot is placed at r_0 and the last at $r_{\max}$[13], and the rest are distributed uniformly along the u radial grid (see Sec. 2.2). The piecewise nature of the splines simplifies the evaluation of integrals, and acts to make the A and S matrices banded, which can typically be solved with high numerical precision.

The basis orbitals are typically defined on a smaller sub-domain of the radial grid. The benefit of restricting the radial sub-domain for the basis is that reasonable completeness can be achieved with fewer basis functions. However, increasing r_0 too much loses the low-r behaviour of the basis orbitals, and making $r_{\max}$ too small loses the correspondence between the "real" and basis orbitals. The ideal choice of sub-domain depends on the specifics of the problem.

Table 2 shows the energies of spline orbitals, using 50 B-splines of order 7 in a cavity of radius $30\,a_B$ with the first internal point at $r = 10^{-5}\,a_B$. This spline basis is orthogonal (or normal) with respect to the Hartree-Fock core to parts in 10^6; the basis itself is orthogonal to parts in 10^{15}. Table 3 shows hyperfine constants calculated using spline orbitals, which is a test of the low-r performance of the orbitals.

5 External fields + matrix elements[14]

5.1 Time-dependent Hartree-Fock

In the presence of a time-varying external field with frequency ω, the orbitals will contain time-varying perturbations:

$$\psi \to \psi + \delta\psi = \psi + Xe^{-i\omega t} + Ye^{i\omega t}, \tag{53}$$

with $\varepsilon \to \varepsilon + \delta\varepsilon$. Keeping terms only to first-order, the corrections are seen to satisfy the equations (e.g., [12]):

$$\begin{aligned} \left(H_{HF} - \varepsilon - \omega\right) X &= -\left(\hat{h} + \delta V - \delta\varepsilon\right)\psi \\ \left(H_{HF} - \varepsilon + \omega\right) Y &= -\left(\hat{h}^\dagger + \delta V^\dagger - \delta\varepsilon\right)\psi, \end{aligned} \tag{54}$$

[13] The actual first knot is placed at 0; the end knots are repeated k times.

[14] Method implemented in: /src/HF/ExternalField.hpp

Table 2: Comparison between energies of spline (DKB) basis orbitals and finite-difference Hartree Fock orbitals. The basis was constructed using 50 B-splines of order 7 in a cavity of radius $30\,a_B$ with the first internal point at $r = 10^{-5}\,a_B$ (only the first 10 splines of each symmetry are shown). Final column shows the root-mean-square radii for the Hartree Fock orbitals. The spline basis energies agree very well (better than parts in 10^6) with the Hartree Fock energies, so long as the cavity is large compared to the typical radius of the orbital in question; for higher orbitals, where this is not the case, the energies diverge significantly. $[\epsilon = (A-B)/A]$

	$s_{1/2}$				$p_{1/2}$			
n	$\varepsilon_{\rm spline}$	$\varepsilon_{\rm HF}$	ϵ	$\langle r^2\rangle^{1/2}_{\rm HF}$	$\varepsilon_{\rm spline}$	$\varepsilon_{\rm HF}$	ϵ	$\langle r^2\rangle^{1/2}_{\rm HF}$
1	−1330.1186542	−1330.1188558	−2e−7	0.03				
2	−212.5644469	−212.5644963	−2e−7	0.12	−199.4294948	−199.4295038	−5e−8	0.10
3	−45.9697097	−45.9697486	−8e−7	0.32	−40.4482937	−40.4483086	−4e−7	0.31
4	−9.5127994	−9.5128206	−2e−6	0.74	−7.4462753	−7.4462846	−1e−6	0.77
5	−1.4898011	−1.4898044	−2e−6	1.88	−0.9078963	−0.9078975	−1e−6	2.15
6	−0.1273679	−0.1273681	−1e−6	6.52	−0.0856153	−0.0856159	−6e−6	8.65
7	−0.055047	−0.0551874	−3e−3	14.58	−0.0411125	−0.0420214	−2e−2	18.16
8	−0.0240059	−0.0309525	−3e−1	25.77	−0.0110954	−0.0251205	−8e−1	30.79
9	0.0147887	−0.0198146		40.11	0.0314743	−0.0167280		46.56
10	0.0679063	−0.0137713		57.61	0.0877553	−0.0119427		65.48

Table 3: Magnetic dipole hyperfine constants A (assuming a point-like nuclear magnetisation distribution), as calculated using the finite-difference Hartree-Fock orbitals, and the DKB basis constructed using 50 B-splines of order 7 in a cavity of radius $50\,a_B$, with varying first internal point (A is sensitive to orbitals at small radial distances). $[\epsilon = (A-B)/A]$

		$r_0 = 10^{-4}\,a_B$		$10^{-5}\,a_B$		$10^{-6}\,a_B$	
n	$A_{\rm HF}$	$A_{\rm Spline}$,	ϵ	$A_{\rm Spline}$,	ϵ	$A_{\rm Spline}$,	ϵ
1	3.9180×10^{7}	3.8361×10^{7}	-2×10^{-2}	3.9172×10^{7}	-2×10^{-4}	3.9179×10^{7}	-3×10^{-6}
2	4.6208×10^{6}	4.5209×10^{6}	-2×10^{-2}	4.6199×10^{6}	-2×10^{-4}	4.6207×10^{6}	-3×10^{-6}
3	9.3463×10^{5}	9.1437×10^{5}	-2×10^{-2}	9.3446×10^{5}	-2×10^{-4}	9.3462×10^{5}	-1×10^{-5}
4	1.9822×10^{5}	1.9392×10^{5}	-2×10^{-2}	1.9819×10^{5}	-2×10^{-4}	1.9823×10^{5}	4×10^{-5}
5	2.7987×10^{4}	2.7380×10^{4}	-2×10^{-2}	2.7982×10^{4}	-2×10^{-4}	2.7988×10^{4}	5×10^{-5}
6	1.4337×10^{3}	1.4022×10^{3}	-2×10^{-2}	1.4334×10^{3}	-2×10^{-4}	1.4336×10^{3}	-4×10^{-5}
7	3.9394×10^{2}	3.8532×10^{2}	-2×10^{-2}	3.9386×10^{2}	-2×10^{-4}	3.9394×10^{2}	-2×10^{-5}
8	1.6448×10^{2}	1.6397×10^{2}	-3×10^{-3}	1.6760×10^{2}	2×10^{-2}	1.6763×10^{2}	2×10^{-2}

where $\hat{h}$ is the tensor operator for the external field with rank k. Here, δV is the correction to the HF potential arising due to the corrections $\{X^{(c)}, Y^{(c)}\}$ to each of the core orbitals, c.

The corrections are not (in general) states of definite angular momentum, but do have definite parity. We expand X and Y in terms of partial waves (χ and η) of definite κ (j^π):

$$\begin{aligned} X^{a,m_a} &= \sum_{\alpha,m_\alpha} X_{\alpha,m_\alpha} \\ &= \sum_{\alpha,m_\alpha} (-1)^{j_\alpha - m_\alpha} \begin{pmatrix} j_\alpha & k & j_a \\ -m_\alpha & q & m_\alpha \end{pmatrix} \chi_{\alpha,m_\alpha}. \end{aligned} \tag{55}$$

The superscript refers to the unperturbed state that X is a correction to (here $a \equiv n_a, \kappa_a$). The sum over α runs over all angular momentum states with $j_\alpha = j_a - k, ..., j_a + k$ and parity $\pi_\alpha = (-1)^{l_a+\pi}$ (where π is the parity of the operator $\hat{h}$). Note that $\{\chi_\alpha\}$ are orthogonal (and are orthogonal to ψ), and form a linearly independent set of solutions to (54).

5.2 Solving the TDHF equations[15]

The δV term in (54) is very important and will be discussed in the next section. Here, we will ignore how it is calculated and just focus on solving the inhomogenous equations.

As before, we express the Hamiltonian as $H = H_{\rm I} + V_{\rm nl}$:

$$H_{\rm I} = H_0 + V_{\rm nuc} + V_{\rm dir} + U_{\rm x} \tag{56}$$
$$V_{\rm nl} = V_{\rm exch} - U_{\rm x}, \tag{57}$$

[15] Functions to solve TDHF equation are in: /src/HF/MixedStates.hpp

where $U_{\rm x}$ is a local approximation to the exchange potential. In the simplest case it is $(f-1)V_{\rm dir}$, but better approximations aid the convergence (we use that from Sec. 3.4). It is desirable to make $V_{\rm nl}$ as small as possible.

We solve the equations iteratively, such that at the nth step:

$$\begin{aligned} (H_{\rm I} - \varepsilon \pm \omega)\, X^{(n)} = \\ -\left(V_{\rm nl}X\right)^{(n-1)} - \left(\hat{h} + \delta V - \delta\varepsilon^{(n-1)}\right)\psi_a, \end{aligned} \tag{58}$$

with $V_{nl}X = 0$ initially. The solution for each α is

$$X_\alpha = \frac{\phi^\infty_\alpha}{cw}\int_0^r \left\{\phi^0_\alpha|S\right\}\, r^2{\rm d}r' + \frac{\phi^0_\alpha}{cw}\int_r^\infty \left\{\phi^\infty_\alpha|S\right\}\, r^2{\rm d}r', \tag{59}$$

where the "source" term S is the rhs of Eq. (58). (Note: the $\delta\varepsilon$ term only contributes for the X term with $\alpha = a$.) The $\phi^{0,\infty}_\varkappa$ functions here are the solutions with Dirac quantum number α to the homogenous equation (19), including both the angular part and the $1/r$. We defined here the "partial" matrix elements, that include only the integral over angular coordinates:

$$\left\{\psi_a|\hat{h}|\psi_b\right\} \equiv \int \psi^\dagger_a \hat{h}\psi_b\,{\rm d}\Omega. \tag{60}$$

We similarly define the partial reduced matrix element:

$$\left\{\psi_a|T^k_q|\psi_b\right\} \equiv (-1)^{j_a-m_a}\begin{pmatrix} j_a & k & j_b \\ -m_a & q & m_b \end{pmatrix}\left\{\psi_a||T^k||\psi_b\right\}. \tag{61}$$

Then, in terms of the partial waves (χ), the solution becomes:

$$\chi_\alpha = \frac{\phi^\infty_\alpha}{cw}\int_0^r \left\{\phi^0_\alpha||S\right\}\, r^2{\rm d}r' + \frac{\phi^0_\alpha}{cw}\int_r^\infty \left\{\phi^\infty_\alpha||S\right\}\, r^2{\rm d}r'. \tag{62}$$

Table 4: Testing TDHF method using Eq. (64) for Cs, with $m = 6p_{1/2}$, $\psi = 6s_{1/2}$ (Hartree-Fock level, no δV).

Operator	(64) lhs	(64) rhs	ϵ^*
$h_{\rm E1}$ $(\omega = \omega_{\rm HF})$	63.2029312	63.2025676	6×10^{-6}
$h_{\rm E1}$ $(\omega = 0)$	126.405501	126.405135	3×10^{-6}
$h_{\rm PNC}$ $(\omega = 0)$	-1.0700928	-1.0700932	4×10^{-7}

$^*\epsilon \equiv (lhs - rhs)/lhs$

This is done so that we only need to calculate the (m-independent) reduced matrix element of $\hat{h}$. The radial integral $|\chi_\alpha|^2$ is used to control convergence (for including the exchange term). Using U_x from Sec. 3.4, convergence (for a given orbital) to parts in 10^9 is typically reached in ~ 10 iterations.

From perturbation theory, the correction (excluding δV and considering the case with $\delta\varepsilon = 0$) can also be expressed as:

$$|X\rangle = \sum_n \frac{|n\rangle\langle n|\hat{h}|\psi\rangle}{\varepsilon - \varepsilon_n + \omega}, \tag{63}$$

which can be used to test the method. Consider, e.g.,

$$\langle m|\chi\rangle = \frac{\langle m||\hat{h}||\psi\rangle}{\varepsilon - \varepsilon_m + \omega}, \tag{64}$$

which can be calculated both ways (lhs vs rhs); see Table 4.

An important application of this technique is that it allows calculations to be done without requiring a summation over the complete set of intermediate states (replaced by solving the inhomogeneous differential equation). This method of performing exact summation over intermediate states is sometimes called the Solving Equations, Mixed States, or Dalgarno-Lewis method [13], depending on context. In this example (64) the intermediate-states summation is trivial, since it involves only single operator and hence only a single intermediate state contributes. In general, all intermediate states (including continuum and positive energy states) contribute, so this method allows calculations without the need for a large basis.

Another way to test the method is to consider the parity non-conservation (PNC) amplitude, which is a correction to the (otherwise forbidden) $E1$ transition between states of the same parity, due to the parity-violating weak interaction between the electrons and nucleus (see, e.g., Ref. [14]). This can be expressed as a sum over all intermediate states n:

$$E^{(z)}_{\rm PNC} = \sum_n \frac{\langle B|\boldsymbol{d}_z|n\rangle\langle n|h_{\rm W}|A\rangle}{\varepsilon_A - \varepsilon_n} + \frac{\langle B|h_{\rm W}|n\rangle\langle n|\boldsymbol{d}_z|A\rangle}{\varepsilon_B - \varepsilon_n}, \tag{65}$$

where $\boldsymbol{d}$ is the $E1$ operator, and $h_{\rm W}$ is the PNC operator. Using the TDHF (Dalgarno-Lewis) method as described in Sec. 5.1, this can also be expressed in two other formally equivalent ways:

$$E^{(z)}_{\rm PNC} = \langle B|\boldsymbol{d}_z|\delta A^{(W)}\rangle + \langle \delta B^{(W)}|\boldsymbol{d}_z|A\rangle \tag{66}$$

$$= \langle \delta B^{(d)}|h_{\rm W}|A\rangle + \langle B|h_{\rm W}|\delta A^{(d)}\rangle, \tag{67}$$

where $\delta A^{(W/d)}$ is the correction to orbital A due to the weak/E1 interaction. Comparing the results of Eqs. (66) and (67) tests the numerical accuracy of the Dalgarno Lewis (solving-equations) method, and comparing these to the result of (65) gives a good test of the basis. The two forms of the Dalgarno Lewis method agree to parts in 10^8. Comparison between the PNC amplitude as calculated using this and the direct-summation method is in Table 5.

Table 5: Comparison of PNC amplitudes (at the HF level) for ^{133}Cs as calculated using the Dalgarno-Lewis (DL) method, and direct summation using a spline basis [formed in a cavity of $(10^{-6}, 50)\,a_B$ using N splines of order k].

		Direct Summation: N/k		
Transition	DL	50/5	60/6	70/7
$6s - 7s$	-0.73954	-0.73948	-0.73953	-0.73954
$6s - 5d_{3/2}$	-2.4000	-2.3998	-2.4000	-2.4000

5.3 Core polarisation (RPA)[16]

This section largely follows Ref. [12] (see also [15–18]). In the presence of an external field, the core electrons become perturbed and a correction to the HF potential is induced, which leads to important corrections to the matrix elements of the external field operator. This effect is often called core polarisation, and is particularly important since it involves corrections with single excitations from the HF core (in the absence of an external field, the lowest-order corrections to the HF potential involve two excitations). The method described here is often referred to as the random phase approximation (RPA).

To account for core polarisation, the set of TDHF equations (54) are solved self-consistently for each of the core orbitals using the method from Sec. 5.1. The δV term is the correction to the HF potential:

$$\delta V = V_{\rm HF}(\{\psi_b + \delta\psi^b\}) - V_{\rm HF}(\{\psi_b\}), \tag{68}$$

where $\{\psi_b\}$ denotes the set of all core orbitals, and the single-particle energy correction is

$$\delta\varepsilon = \langle\psi_b|\hat{h} + \delta V|\psi_b\rangle. \tag{69}$$

The TDHF equations are solved iteratively, updating the δV and $\delta\varepsilon$ terms at each step until convergence is reached; i.e., at the nth step, we have

$$(H_{\rm HF} - \varepsilon - \omega)\, X^{(n)}_\beta = -\left(\hat{h} + \delta V^{(n-1)} - \delta\varepsilon^{(n-1)}\right)\psi_b, \tag{70}$$

with $\delta V = 0$ for the initial iteration (similar for Y). After integrating over angles, the $\delta\varepsilon$ term only appears in the equations when $\beta = b$, which for odd-parity operators is never the case.

Combining Eqs. (68) with (28), we have:

$$\begin{aligned}\delta V\phi_a(\boldsymbol{r}_1) = \sum_{i\neq a}^{N_c}\Bigg(&\int \frac{\phi^\dagger_i(\boldsymbol{r}_2)X^i(\boldsymbol{r}_2)}{|\boldsymbol{r}_{12}|}\mathrm{d}^3\boldsymbol{r}_2\,\phi_a(\boldsymbol{r}_1)\\ &+\int \frac{Y^{i\dagger}(\boldsymbol{r}_2)\phi_i(\boldsymbol{r}_2)}{|\boldsymbol{r}_{12}|}\mathrm{d}^3\boldsymbol{r}_2\,\phi_a(\boldsymbol{r}_1)\\ &-\int \frac{\phi^\dagger_i(\boldsymbol{r}_2)\phi_a(\boldsymbol{r}_2)}{|\boldsymbol{r}_{12}|}\mathrm{d}^3\boldsymbol{r}_2\,X^i(\boldsymbol{r}_1)\\ &-\int \frac{Y^{i\dagger}(\boldsymbol{r}_2)\phi_a(\boldsymbol{r}_2)}{|\boldsymbol{r}_{12}|}\mathrm{d}^3\boldsymbol{r}_2\,\phi_i(\boldsymbol{r}_1)\Bigg),\end{aligned} \tag{71}$$

[16] Method implemented in: /src/HF/ExternalField.hpp

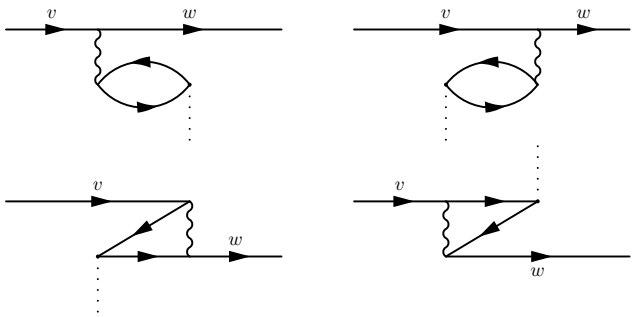

Figure 4: Diagrams representing the lowest order direct and exchange core-polarisation (RPA) corrections to the $\langle w|\hat{h}|v\rangle$ amplitude. Wavy line is Columb interaction, dotted line is external field ($\hat{h}$). All internal lines are summed over: forwards lines are virtual excited states, backward lines are holes in the core. In higher-order diagrams, each $\hat{h}$ vertex is corrected again by these four diagrams (RPA).

using notation of Eq. (55). The reduced matrix elements are:

$$\langle\phi_n||\delta V||\phi_a\rangle = \sum_{b\beta}\left(\frac{C^k_{na}C^k_{\beta b}}{[k]}(R^k_{nba\beta}+R^k_{nba\beta'})\right.$$
$$-(-1)^{j_\beta-j_a}\sum_\lambda(-1)^{k+\lambda}\left[C^\lambda_{ab}C^\lambda_{n\beta}\begin{Bmatrix} j_a & j_n & k\\ j_\beta & j_b & \lambda\end{Bmatrix}R^\lambda_{na\beta b}\right.$$
$$\left.\left.+C^\lambda_{a\beta}C^\lambda_{nb}\begin{Bmatrix} j_a & j_n & k\\ j_b & j_\beta & \lambda\end{Bmatrix}R^\lambda_{nab\beta'}\right]\right), \quad (72)$$

where the sum b runs over all core orbitals, and β runs over all (partial wave) corrections to b. The prime (β') means the η_β orbital is used; no prime means χ_β. The equation for $\langle\phi_n||\delta V^\dagger||\phi_a\rangle$ is the same, but with $\beta\leftrightarrow\beta'$. For the radial equation for δVF_a (corresponding to angular momentum state κ_n), make substitution: $R^k_{abcd}\to y^k_{bd}F_c$. Here,

$$R^k_{abcd}\equiv\int \mathrm{d}r_1\,\left[f_a(r_1)f_c(r_1)+g_a(r_1)g_c(r_1)\right]\,y^k_{bd}(r_1), \quad (73)$$

and y^k_{bd} and C^k_{ab} are given by Eqs. (31) and (32).

In this method, matrix elements of the operator $\hat{h}$ between valence states v and w are calculated including the effect of core polarisation as [12]

$$\langle w|\hat{h}+\delta V|v\rangle, \quad (74)$$

which is equivalent to the RPA method (see, e.g., Ref. [3]). If the equations (70) are solved just once (without iterations), it corresponds to the lowest (first) order correction to the amplitude, which are shown in Fig. 4. Further iterations correspond to higher-orders. By continuing the iterations until convergence is reached, core polarisation is included to all-orders.

Core polarisation can by included into the Dalgarno-Lewis method for exact summation over intermediate states by solving the equation (54) for the required valence states (including the δV, which must be found first).

5.3.1 Algebraic method

The THDF equations can also be solved using an algebraic method, by expanding the χ and η corrections over a basis of states:

$$\chi^{\varkappa}=\sum_j a_j x_j\,,\qquad \eta^{\varkappa}=\sum_j b_j x_j\,, \quad (75)$$

where $\{x_j\}$ is the set of basis orbitals, and $\{a_j/b_j\}$ are the expansion coefficients. Multiply Eq. (54) from the left by $x^\dagger_i$ (and integrate), which yields the matrix equations:

$$\begin{aligned}[H_{ij}-(\varepsilon-\omega)S_{ij}]\,a_j &= -h_{ic}-\delta V_{ic}+\delta\varepsilon_c S_{ic}\delta_{\kappa_i\kappa_c}\\ [H_{ij}-(\varepsilon+\omega)S_{ij}]\,b_j &= -h^\dagger_{ic}-\delta V^\dagger_{ic}+\delta\varepsilon_c S_{ic}\delta_{\kappa_i\kappa_c}.\end{aligned} \quad (76)$$

Here,

$$\begin{aligned}H_{ij}&=\langle x_i|\hat{H}_{\rm HF}|x_j\rangle\,, & S_{ij}&=\langle x_i|x_j\rangle\,,\\ h_{ic}&=\langle x_i||\hat{h}||\psi_c\rangle\,, & \delta\varepsilon_c&=\langle\psi_c||\hat{h}+\delta V||\psi_c\rangle,\end{aligned} \quad (77)$$

δV_{ic} is given by Eq. (72), and the delta function means the $\delta\varepsilon$ term only appears for partial-wave corrections with $\kappa=\kappa_c$.

There are two ways to proceed. The simplest way is to solve (76), which is a pair of linear matrix equations, for the set of expansion coefficients, a_j and b_j. This must be solved for each partial wave correction ($\varkappa_i$) to each core state c. Note, however, that δV depends on the corrected states, and thus on a and b; so this would have to be solved iteratively. In another approach, the δV term is also expanded in terms of the basis; then no iterations are required, and the equations take the form of a generalised eigenvalue problem, see Ref. [18].

5.4 Core polarisation (RPA diagram technique)[17]

The core polarisation correction to a matrix element can also be taken into account by directly evaluating the four diagrams in Fig. 4. To lowest order, the matrix element of operator $\hat{h}$ is $h^{(0)}_{ij}$. The first-order correction is then [2]:

$$\delta h_{ij}=\sum_{ma}\frac{h^{(0)}_{am}\widetilde{g}_{imja}}{\varepsilon_a-\varepsilon_m-\omega}+\sum_{ma}\frac{h^{(0)}_{ma}\widetilde{g}_{iajm}}{\varepsilon_a-\varepsilon_m+\omega}, \quad (78)$$

where $\widetilde{g}_{abcd}=g_{abcd}-g_{abdc}$, with g_{abcd} being the two-electron Coulomb matrix element (see appendix for definition). The a sum runs over all occupied core electrons (n,κ,m), while m runs over all virtual excited states.

In the RPA method, the lowest-order matrix elements in δh_{ij} (78) are then replaced with the corrected values. This process is repeated iteratively (for all core states i and j) until convergence is reached; i.e., at the nth iteration we have:

$$\delta h^n_{ij}=\sum_{ma}\left(\frac{(h^{(0)}_{am}+\delta h^{n-1}_{am})\widetilde{g}_{imja}}{\varepsilon_a-\varepsilon_m-\omega}+\frac{(h^{(0)}_{ma}+\delta h^{n-1}_{ma})\widetilde{g}_{iajm}}{\varepsilon_a-\varepsilon_m+\omega}\right). \quad (79)$$

The reduced matrix element in the RPA approach is then:

$$\langle i||h||j\rangle^{\rm RPA}=\langle i||h||j\rangle+\langle i||\delta h||j\rangle, \quad (80)$$

with

$$\langle i||\delta h||j\rangle=\frac{1}{[k]}\sum_{am}(-1)^{j_a-j_i+k}\left(\frac{\langle a||t||m\rangle^{\rm RPA}W^k_{imja}}{\varepsilon_a-\varepsilon_m-\omega}\right.$$
$$\left.+(-1)^{j_a-j_m}\frac{\langle m||t||a\rangle^{\rm RPA}W^k_{iajm}}{\varepsilon_a-\varepsilon_m+\omega}\right), \quad (81)$$

(see appendix for W^k_{abcd} definition; sum is now over orbitals n,κ). RPA matrix elements between valence states have the same expression (the equations need only be iterated for the core electrons). Note that W depends only on the *rank* of the operator, so in theory, they need only be calculated once. In practise, we only calculate W^k_{imja} (e.g.), when $t_{am}\neq 0$ – meaning effectively that W also depends on the operator parity.

[17] Method implemented in: /src/MBPT/DiagramRPA.hpp

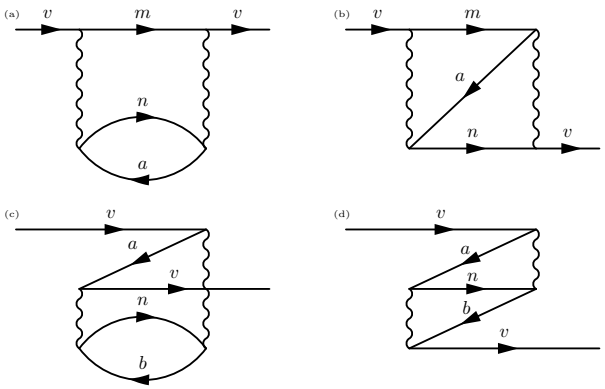

Figure 5: Goldstone diagrams for the second-order correlation correction to the energy for valence state v. Backward facing lines denote (single-particle) states in the core; n and m are virtual excited states. Diagrams (a) and (c) are direct diagrams, (b) and (d) are corresponding exchange diagrams.

6 Correlation corrections[18]

Correlation corrections are the deviation from the pure single-particle picture, and correspond to many-body effects beyond the mean field (Hartree Fock) approximation. The many-body atomic Hamiltonian may be expressed as

$$H = \sum_i h_{\rm HF}(\boldsymbol{r}_i) + \delta V_{\rm corr}, \tag{82}$$

where $h_{\rm HF}(\boldsymbol{r}_i)$ is the single-particle HF Hamiltonian (27), and

$$\delta V_{\rm corr} = \sum_{i<j} \frac{1}{\boldsymbol{r}_{ij}} - \sum_i V_{\rm HF}(\boldsymbol{r}_i) \tag{83}$$

is the *residual Coulomb interaction* (beyond the mean potential) that may be taken into account perturbatively. We consider the case of an atom with a single valence electron (v) above closed shells. In the single particle picture, this perturbation corresponds to residual interactions of the valence electron with the indevidual electrons in the core. Starting from the Hartree-Fock method with a V^{N-1} potential, there are no first-order corrections to the wavefunction (that is, corrections involving a single core excitation) [2].

Notation: In this section (and elsewhere), I use the convention that letters at the beginning of the alphabet (a, b, ...) denote occupied core states (or holes), those from the middle (n, m, ...) denote virtual excited states, and those from the end (v, w, ...) denote valence states. The letters (i, j, ...) are dummy indices that may stand for any state.

6.1 Second-order correlations: Goldstone technique

This section follows closely the method from Ref. [12]. Goldstone diagrams for the second-order correction to the valence energy are shown in Fig. 5. This can be expressed as [3, 12]:

$$\delta E_v = \sum_{amn} \frac{g_{vamn}\widetilde{g}_{nmav}}{\varepsilon_v + \varepsilon_a - \varepsilon_m - \varepsilon_n} + \sum_{abn} \frac{g_{vnab}\widetilde{g}_{banv}}{\varepsilon_v + \varepsilon_n - \varepsilon_a - \varepsilon_b}, \tag{84}$$

where m and n run over (unoccupied) virtual excited states, and a and b run over (occupied) core states (there is an implicit sum over magnetic quantum numbers here). The first term corresponds to the diagrams (a) and (b), the second to (c) and (d) [Fig. 5]. Here, $\widetilde{g}_{abcd} = g_{abcd} - g_{abdc}$ is the anti-symmetrised Coulomb integral (i.e., accounting for exchange), with

$$g_{abcd} = \sum_{kq} (-1)^q \langle a_{\kappa m}|C^k_{-q}|c_{\kappa m}\rangle \langle b_{\kappa m}|C^k_q|d_{\kappa m}\rangle R^k_{abcd}. \tag{85}$$

Summing over magnetic quantum numbers, this gives [12]

$$\delta E_v = \sum_k \frac{1}{[k][j_v]} \left(\sum_{amn} \frac{Q^k_{vamn} W^k_{vamn}}{\varepsilon_v + \varepsilon_a - \varepsilon_m - \varepsilon_n} + \sum_{abn} \frac{Q^k_{vnba} W^k_{vnba}}{\varepsilon_v + \varepsilon_n - \varepsilon_b - \varepsilon_a} \right), \tag{86}$$

where we made use of symmetries,

$$Q^k_{abcd} \equiv (-1)^k \widetilde{C}^k_{ac} \widetilde{C}^k_{bd} R^k_{abcd}, \tag{87}$$

$$W^k_{abcd} \equiv Q^k_{abcd} + [k] \sum_\lambda \begin{Bmatrix} j_a & j_c & k \\ j_b & j_d & \lambda \end{Bmatrix} Q^\lambda_{abdc}, \tag{88}$$

and $\widetilde{C}^k_{ab} \equiv (-1)^{j_a+1/2} C^k_{ab}$.[19] Note that W may be further broken into two terms: $W^k_{abcd} = Q^k_{abcd} + P^k_{abcd}$, where Q corresponds to the direct term, and P corresponds to exchange. For the angular reduction, we used the identities (see appendix):

$$\sum_{m_{i,j,k,l}} g_{ijkl}\, g_{lkji} = \sum_\mu \frac{1}{[\mu]} \left(Q^\mu_{ijkl}\right)^2 \tag{89}$$

$$\sum_{m_{i,j,k,l}} g_{ijkl}\, g_{klji} = -\sum_\mu \frac{1}{[\mu]} Q^\mu_{ijkl} P^\mu_{ijkl}. \tag{90}$$

We define the *correlation potential*, $\hat{\Sigma}$, defined so that its matrix elements correspond to the energy shift: $\langle v|\Sigma^{(2)}|v\rangle = \delta E_v$. We define $Q^{k(\kappa_v)}_{nba}(r)$ (which we will write as $Q^{k(v)}_{nba}$ for brevity, though note it depends only on κ_v and not F_v), via:

$$Q^k_{vnba} = \langle F_v|Q^{k(v)}_{nba}\rangle = \int F_v(r)\, Q^{k(v)}_{nba}(r)\, {\rm d}r. \tag{91}$$

Note that $Q^{k(v)}_{nba}$ has the form of a radial Dirac spinor [Eq. (8)]. Then, we may express the (energy dependent) second-order correlation potential as

$$\hat{\Sigma}^{(2)}_\varepsilon = \sum_{kabnm} \frac{1}{[k][j_v]} \left(\frac{|Q^{k(v)}_{amn}\rangle\langle W^{k(v)}_{amn}|}{\varepsilon + \varepsilon_a - \varepsilon_m - \varepsilon_n} + \frac{|Q^{k(v)}_{nba}\rangle\langle W^{k(v)}_{nba}|}{\varepsilon + \varepsilon_n - \varepsilon_b - \varepsilon_a} \right), \tag{92}$$

which is sometimes called the self-energy operator. This has the form of a sum of operators,

$$\hat{G}^{(v)}_{nba}(\varepsilon) = \sum_k \frac{1}{[k][j_v]} \frac{|Q^{k(v)}_{nba}\rangle\langle W^{k(v)}_{nba}|}{\varepsilon + \varepsilon_n - \varepsilon_b - \varepsilon_a}, \tag{93}$$

which can be expressed in (radial) coordinate space as

$$G^{(v)}_{nba}(r_1, r_2, \varepsilon) = \sum_k \frac{1}{[k][j_v]} \frac{Q^{k(v)}_{nba}(r_1)\, W^{k(v)}_{nba}(r_2)}{\varepsilon + \varepsilon_n - \varepsilon_b - \varepsilon_a}. \tag{94}$$

Thus the correlation potential may be expressed as

$$\Sigma^{(2)}_\varepsilon(r_1, r_2) = \sum_{abnm} \left[G^{(v)}_{amn}(r_1, r_2, \varepsilon) + G^{(v)}_{nba}(r_1, r_2, \varepsilon) \right]. \tag{95}$$

[18] Method implemented in: /src/MBPT/CorrelationPotential.hpp

[19] Note: Q^k here differs from that defined in, e.g., Ref. [12] by a factor of ± 1; our definition is chosen due to the symmetry properties; see appendix.

Note that Σ is a matrix in (radial) spinor space:

$$\Sigma \propto \begin{pmatrix} f_Q(r_1)f_W(r_2) & f_Q(r_1)g_W(r_2) \\ g_Q(r_1)f_W(r_2) & g_Q(r_1)g_W(r_2) \end{pmatrix}, \tag{96}$$

where f and g are the large and small components of the Q/W radial spinors. Each of these four terms can themselves be represented as square matrices (on a radial grid). It is common to only calculate the first (ff) term; it is also common to store the Σ matrix on only a subset of the radial grid.

6.2 Correlation potential method (Brueckner orbitals)

In the *correlation potential method* [20, 21], the non-local energy-dependent Σ operator is added to the single-particle Hartree Fock equation for the valence states:

$$(H_{\rm HF} + \hat{\Sigma}_\varepsilon)\psi^{\rm (Br)} = \varepsilon^{\rm (Br)}\psi^{\rm (Br)}. \tag{97}$$

The resulting orbitals are known as Brueckner orbitals[20], which include the dominating second-order correlation effects. This means, for example, the dominant correlation corrections can be included into the calculation of matrix elements simply by using the Brueckner orbitals, e.g., $\langle a^{\rm HF}|\hat{v}|b^{\rm HF}\rangle \to \langle a^{\rm Br}|\hat{v}|b^{\rm Br}\rangle$. We will drop the (Br) superscript from here on unless it is necessary to avoid confusion. The iterations of the Hartree Fock equation for the valence state actually means that certain classes of diagrams are included to all orders; this is called the *chaining* of the self-energy operator. Calculations using the second-order correlation potential method for energies of the lowest states of the alkali atoms are presented in Table 6.

The Σ operator should be evaluated at the Hartree Fock energy of the valence state. However, in order to maintain the orthogonality of the orbitals, all orbitals of the same angular momentum and parity must see the exact same potential. Therefore, for each κ, the correlation potential Σ must be evaluated at the same energy. Typically, this is taken as the Hartree-Fock value of the energy of the lowest valence state v of the given symmetry (since this is typically where the highest accuracy is required, and because the correlation corrections are larger for lower states). Note also that since $|\varepsilon_n| \gg |\varepsilon_v|$, the correlation potential depends only weakly on ε_v [see Eq. (84)].

To estimate the effect of higher-order correlations, one may introduce scaling factors for the correlation potential, i.e., $\Sigma \to \lambda\Sigma$ in Eq. (97), which are chosen to reproduce the removal energies for the lowest-lying valence states. For Cs, $\lambda \approx 0.82$ for s and 0.86 p states. This semi-empirical addition leads to much improved agreement with experiment. See Table 7 for a summary of calculations of electric dipole ($E1$) matrix elements for Cs, and Table 8 for calculated lifetimes.

One may also include the correlation corrections into a set of basis orbitals by adding the correlation potential to the Hartree Fock Hamiltonian when solving the eigenvalue problem for the set of B-splines; i.e.,

$$H_{ij} \to \langle S_i|\hat{H}_{\rm HF}|S_j\rangle + \langle S_i|\hat{\Sigma}_\varepsilon|S_j\rangle \tag{98}$$

in Eq. (50). This leads to an (approximately) complete set of orbitals that include correlation effects. These orbitals may then be used in calculations requiring a summation of a complete set of orbitals; so this method allows the inclusion of correlation corrections into such calculations in a reasonably simple way. Note that this apprach will lead to a set of orbitals corresponding to orbitals in the core; however, due to the presence of the Σ operator, these orbitals will not be orthogonal to the Hartree Fock core orbitals. These "core" orbitals are required for the completeness of the set, and should be included in such summations.

The correlation potential can also be taken into account in the time-dependent Hartree Fock method for the valence state:

$$\Big(H_{HF} + \hat{\Sigma}_\varepsilon - \varepsilon - \omega\Big)\,X = -\Big(\hat{h} + \delta V - \delta\varepsilon\Big)\,\psi_v. \tag{99}$$

This gives a means of including the correlation corrections into the Dalgarno-Lewis (Mixed States/Solving Equations) method. Note that δV here is the usual core polarisation correction; the Σ operator should not be included into the self-consistent TDHF equations for the core.

7 Correlation potential: Feynman method

This section describes the method as developed in Ref. [25], and follows that work closely; see also [26–28]. Where necessary, I will include subscripts on the Dirac bra/kets to indicate which coordinate they belong to. I will also abuse the Dirac notation in this section so that $|a\rangle_1$ is just a short-hand for $\phi_a(\boldsymbol{r}_1)$; note that when the coordinate index is shown, there is no implied integration in the "braket", e.g.:

$$\langle a|_1|b\rangle_1 = \phi^\dagger_a(\boldsymbol{r}_1)\phi_b(\boldsymbol{r}_1), \quad \text{while} \quad \langle a|b\rangle = \int \mathrm{d}^3\boldsymbol{r}'\phi^\dagger_a(\boldsymbol{r}')\phi_b(\boldsymbol{r}').$$

7.1 Feynman Green's function

First, we introduce the Feynman Green's function, which can be expressed as (see [25, 26] and references therein):

$$\hat{G}(\varepsilon) = \lim_{\delta\to 0}\left(\sum_a^{\rm core}\frac{|a\rangle\langle a|}{\varepsilon - \varepsilon_a - i\delta} + \sum_n^{\rm exc.}\frac{|n\rangle\langle n|}{\varepsilon - \varepsilon_n + i\delta}\right). \tag{100}$$

Note that, if ε is the (single-particle) ground-state energy, $\varepsilon > \varepsilon_a$, but $\varepsilon < \varepsilon_n$. Conceptually, the simplest way to evaluate it is by summation over the complete set of core and excited orbitals using a pseudospectrum basis as described previously. It is also, however, possible to evaluate the Green's function exactly (up to numerical errors) without the need for a basis.

Consider the inhomogeneous Dirac equation including exchange, and its homogeneous counterpart (without exchange):

$$(H_0 + V_{\rm d} - \varepsilon)\phi = -V_{\rm x}\phi \tag{101}$$
$$(H_0 + V_{\rm d} - \varepsilon)\chi = 0 \tag{102}$$

with χ_0 being the homogeneous solution regular at the origin, and χ_∞ that regular at infinity. The local Green's function (without exchange) can be expressed in coordinate space as:

$$\hat{G}_0 \equiv G_0(\boldsymbol{r}_1, \boldsymbol{r}_2) = \frac{\chi_0(r_<, \hat{\boldsymbol{n}})\chi_\infty(r_>, \hat{\boldsymbol{n}})}{w}, \tag{103}$$

where $r_< = \min(r_1, r_2)$, and $w = (f_0 g_\infty - f_\infty g_0)/\alpha$ (w is independent of r, and f, g are radial components of χ). Exchange can be taken into account by solving the Dyson equation [26, 27]

$$\hat{G} = \hat{G}_0 + \hat{G}_0\hat{V}_{\rm x}\hat{G} = \Big[1 - \hat{G}_0\hat{V}_{\rm x}\Big]^{-1}\hat{G}_0. \tag{104}$$

[20] Note that the exact definition of "Brueckner" orbitals varies slightly depending on the source; we use the definition from [20].

Table 6: Removal energies for the lowest s, p, and d states for the alkali atoms as calculated with the Hartree-Fock and second-order correlation potential methods, and comparison with experiment (Ref. [19]). Note: Calculation of Σ used only basis states up to $l = 4$; states up to $l = 6$ are important, especially for heavy atoms, so these should be taken as an example only. The inclusion of the correlation potential greatly improves the accuracy of the calculations.

	Expt.	HF		$\Sigma^{(2)}$			Expt.	HF		$\Sigma^{(2)}$	
Li ($Z=3$)						Rb ($Z=37$)					
$2s_{1/2}$	−43487.1	−43087.3	−0.9%	−43450.6	−0.08%	$5s_{1/2}$	−33690.8	−30570.9	−9.3%	−34162.9	1.4%
$2p_{1/2}$	−28583.5	−28232.9	−1.2%	−28539.3	−0.15%	$5p_{1/2}$	−21111.9	−19931.8	−5.6%	−21231.3	0.6%
$2p_{3/2}$	−28583.1	−28232.3	−1.2%	−28538.7	−0.16%	$5p_{3/2}$	−20874.3	−19749.6	−5.4%	−20982.4	0.5%
$3d_{3/2}$	−12204.0	−12194.4	−0.08%	−12208.3	0.04%	$4d_{3/2}$	−14335.6	−13112.5	−8.5%	−14415.9	0.6%
$3d_{5/2}$	−12204.0	−12194.4	−0.08%	−12208.3	0.04%	$4d_{5/2}$	−14335.2	−13099.7	−8.6%	−14411.7	0.5%
Na ($Z=11$)						Cs ($Z=55$)					
$3s_{1/2}$	−41449.5	−39951.5	−3.6%	−41272.7	−0.4%	$6s_{1/2}$	−31406.5	−27954.1	−11.0%	−32289.8	2.8%
$3p_{1/2}$	−24493.3	−24030.4	−1.9%	−24427.8	−0.3%	$6p_{1/2}$	−20228.2	−18790.5	−7.1%	−20488.3	1.3%
$3p_{3/2}$	−24476.1	−24014.1	−1.9%	−24409.6	−0.3%	$6p_{3/2}$	−19674.2	−18388.8	−6.5%	−19894.6	1.1%
$3d_{5/2}$	−12276.6	−12217.4	−0.5%	−12267.5	−0.07%	$5d_{5/2}$	−16907.2	−14162.6	−16.2%	−17230.9	1.9%
$3d_{3/2}$	−12276.6	−12217.4	−0.5%	−12267.4	−0.07%	$5d_{3/2}$	−16809.6	−14138.5	−15.9%	−17090.5	1.7%
K ($Z=19$)						Fr ($Z=87$)					
$4s_{1/2}$	−35009.8	−32370.4	−7.5%	−35316.2	0.9%	$7s_{1/2}$	−32848.9	−28767.1	−12.4%	−33944.4	3.3%
$4p_{1/2}$	−22024.6	−21006.5	−4.6%	−22097.1	0.3%	$7p_{1/2}$	−20611.5	−18855.2	−8.5%	−20928.5	1.5%
$4p_{3/2}$	−21966.9	−20959.4	−4.6%	−22036.1	0.3%	$7p_{3/2}$	−18924.9	−17655.3	−6.7%	−19124.5	1.1%
$3d_{5/2}$	−13475.1	−12747.0	−5.4%	−13516.3	0.3%	$6d_{3/2}$	−16619.0	−13924.5	−16.2%	−16872.6	1.5%
$3d_{3/2}$	−13472.8	−12744.3	−5.4%	−13514.6	0.3%	$6d_{5/2}$	−16419.2	−13825.5	−15.8%		

Table 7: Reduced $E1$ matrix elements (absolute values) for transitions between the lowest states for Cs as calculated in different approximations, and comparison with experiment (experimental values taken from Ref. [22]). RPA means including core-polarisation, Σ means using second-order Brueckner orbitals (including core polarisation), and $\lambda\Sigma$ means Brueckner orbitals calculated using scaled correlation potential.

	HF	RPA	$\Sigma^{(2)}$	$\lambda\Sigma^{(2)}$	Expt.
$6s-6p_{1/2}$	5.278	4.975	4.404	4.5047	4.5057(16)
$6s-6p_{3/2}$	7.426	7.014	6.193	6.3399	6.3398(22)
$6s-7p_{1/2}$	0.3717	0.2382	0.2996	0.2750	0.2781(44)
$6s-7p_{3/2}$	0.6947	0.5083	0.6049	0.5694	0.5742(57)
$7s-6p_{1/2}$	4.413	4.450	4.234	4.240	4.249(40)
$7s-6p_{3/2}$	6.671	6.713	6.483	6.475	6.489(50)

Table 8: Calculated lifetimes of the lowest states of Cs in various approximations, and comparison with experiment. Note that calculated frequencies, not experimental values, are used for the HF, RPA and $\Sigma^{(2)}$; since lifetimes scale as ω^3, this is the leading source of error. Experimental results tabulated in Ref. [23], except for $5d_{5/2}$ which is from Ref. [24].

	HF	RPA	$\Sigma^{(2)}$	$\lambda\Sigma^{(2)}$	Expt.	Other†
$6p_{1/2}$	46.1	51.8	31.0	34.83	34.934(94)	34.4(12)
$6p_{3/2}$	40.9	45.9	27.0	30.42	30.460(38)	30.0(7)
$5d_{3/2}$	210.4	227.1	1077.2	966.78	909(15)	966(34)
$5d_{5/2}$	264.2	284.0	1494.6	1348.3	1353(5)	1351(52)

† Theory (CCSDpT) calculations from Ref. [23]

The local direct and non-local exchange operators are

$$\hat{V}_{\rm d} = \sum_a^{\rm core} \langle a|\hat{Q}|a\rangle, \quad \text{and} \quad \hat{V}_{\rm x} = -\sum_a^{\rm core} |a\rangle\hat{Q}\langle a|, \tag{105}$$

respectively, with the (two-particle) Coulomb operator:

$$\hat{Q}(\boldsymbol{r}_1,\boldsymbol{r}_2) = \boldsymbol{r}_{12}^{-1}. \tag{106}$$

These operators may be represented as coordinate matrices: e.g., $\hat{G} \Leftrightarrow G(\boldsymbol{r}_1,\boldsymbol{r}_2)$. Multiplication is understood to mean:

$$\hat{W} = \hat{X}\hat{Y}\hat{Z} \Rightarrow W(r_1,r_2) = \iint \mathrm{d}r_i \mathrm{d}r_j X(r_1,r_i)Y(r_i,r_j)Z(r_j,r_2).$$

Note how the 'hat' notation is used. Note also that G, Q, V etc. are symmetric.

7.2 Two useful integrals

Here, I present two useful analytic integrals involving Feynman Green's functions. These are evaluated analytically by extending the integral over the complex plane. As a reminder, Cauchy's integral formula is

$$\oint \mathrm{d}z \frac{f(z)}{z-a} = 2\pi i f(a).$$

The first integral[21]

$$\int \frac{\mathrm{d}\omega}{2\pi} \hat{G}_{12}(\varepsilon_i+\omega)\hat{G}_{34}(\varepsilon_j+\omega) \tag{107}$$

$$= \sum_{abnm} \int \frac{\mathrm{d}\omega}{2\pi} \left(\frac{|a\rangle_1\langle a|_2}{\varepsilon_i+\omega-\varepsilon_a-i\delta} + \frac{|n\rangle_1\langle n|_2}{\varepsilon_i+\omega-\varepsilon_n+i\delta} \right) \times \left(\frac{|b\rangle_3\langle b|_4}{\varepsilon_j+\omega-\varepsilon_b-i\delta} + \frac{|m\rangle_3\langle m|_4}{\varepsilon_j+\omega-\varepsilon_m+i\delta} \right), \tag{108}$$

can be expanded to four seperate terms, each with a pair of poles. Consider the first ("a,b") term of (108):

$$\int \frac{\mathrm{d}\omega}{2\pi} \left(\frac{|a\rangle\langle a|}{\varepsilon_i+\omega-\varepsilon_a-i\delta} \right) \left(\frac{|b\rangle\langle b|}{\varepsilon_j+\omega-\varepsilon_b-i\delta} \right), \tag{109}$$

[21] Note $|G(\omega)| \to 0$ as $|\omega| \to \infty$ ($\omega \in \mathbb{C}$); see Eq. (100).

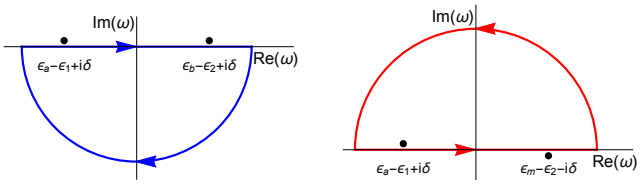

Figure 6: Contours for the "a, b" and "a, m" terms of Eq. (108).

which has poles at $\omega = \varepsilon_{a/b} - \epsilon_{i/j} + i\delta$. By closing the contour in the lower complex plane, see Fig. 6 (left), it is seen the integral is zero. The same is found for the last ("n, m") term by closing the contour in the upper plane. The other two terms are non-zero, and can be evaluated by closing the contour in the upper plane; an example for the "a, m" term with pole at $\omega = \varepsilon_a - \varepsilon_i + i\delta$ is given in Fig. 6 (right). Together, this gives the final expression:[22]

$$\int \frac{\mathrm{d}\omega}{2\pi}\hat{G}_{12}(\varepsilon_i+\omega)\hat{G}_{34}(\varepsilon_j+\omega) = i\sum_{an}\left[\frac{|a\rangle_1\langle a|_2\,|n\rangle_3\langle n|_4}{\varepsilon_j-\varepsilon_i+\varepsilon_a-\varepsilon_n} + \frac{|n\rangle_1\langle n|_2\,|a\rangle_3\langle a|_4}{\varepsilon_i-\varepsilon_j+\varepsilon_a-\varepsilon_n}\right]. \quad (110)$$

The second integral is found in the same way:

$$\int \frac{\mathrm{d}\omega}{2\pi}\hat{G}_{12}(\varepsilon_i+\omega)\hat{G}_{34}(\varepsilon_j-\omega) = i\sum_{abnm}\left[\frac{|a\rangle_1\langle a|_2\,|b\rangle_3\langle b|_4}{\varepsilon_i+\varepsilon_j-\varepsilon_a-\varepsilon_b} - \frac{|n\rangle_1\langle n|_2\,|m\rangle_3\langle m|_4}{\varepsilon_i+\varepsilon_j-\varepsilon_m-\varepsilon_n}\right]. \quad (111)$$

7.3 Feynman method for second-order correlations

In the Feynman technique, the second-order correlation corrections are given by the diagrams presented in Fig. 7. The straight lines represent Hartree-Fock (bound-electron) Green's functions (100), the wavy photon lines represent the Coulomb operator (106), and the electron loops represent the polarisation operator:

$$\hat{\Pi}_{12}(\omega) = \int \frac{\mathrm{d}\varepsilon'}{2\pi}\hat{G}_{12}(\varepsilon')\hat{G}_{21}(\omega+\varepsilon'). \quad (112)$$

Note that this is a (largely) non-relativistic many-body problem; the polarisation is of the atomic core, not the vacuum.

Using Eq. (110), the integral over frequencies in the polarisation operator can be performed analytically, yielding:

$$\hat{\Pi}(\omega) = i\sum_{an}\left[\frac{|a\rangle_2\langle a|_1\,|n\rangle_1\langle n|_2}{\varepsilon_a-\omega-\varepsilon_n} + \frac{|n\rangle_2\langle n|_1\,|a\rangle_1\langle a|_2}{\varepsilon_a+\omega-\varepsilon_n}\right], \quad (113)$$

which can be further simplified to:

$$\hat{\Pi}(\omega) = i\sum_{a}|a\rangle\left[\hat{G}^{\mathrm{ex}}(\varepsilon_a-\omega)+\hat{G}^{\mathrm{ex}}(\varepsilon_a+\omega)\right]\langle a|. \quad (114)$$

Here, $\hat{G}^{\mathrm{ex}}$ only includes excited orbitals. It can be formed without the use of a basis using Eqs. (104) and (100), so long as the core orbitals are known. In practise, it is numerically unstable to calculate $\hat{G}^{\mathrm{ex}} = \hat{G} - \hat{G}^{\mathrm{core}}$; instead, we compute:

$$\hat{G}^{\mathrm{ex}} = \hat{G} - \sum_{a}^{\mathrm{core}}|a\rangle\langle a|\hat{G}. \quad (115)$$

[22] I renamed $m = n$ in the first term, and $b = a$ in the second.

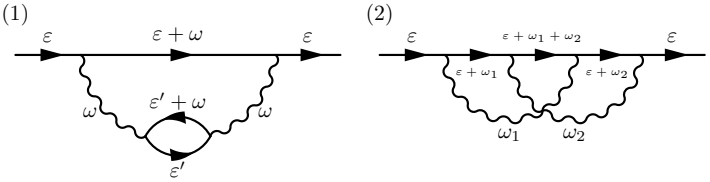

Figure 7: Second-order direct (1) and exchange (2) correlation diagrams in the Feynman technique.

With these, the direct (d) and exchange (x) correlation potentials can be expressed in the Feynman approach as

$$\hat{\Sigma}^{(2)}_{\mathrm{d}} = \iint \mathrm{d}^3r_i\mathrm{d}^3r_j\int\frac{\mathrm{d}\omega}{2\pi}\hat{G}_{12}(\varepsilon+\omega)\hat{Q}_{1i}\hat{\Pi}_{ij}(\omega)\hat{Q}_{j2}, \quad (116)$$

and

$$\hat{\Sigma}^{(2)}_{\mathrm{x}} = -\iint \mathrm{d}^3r_i\mathrm{d}^3r_j\iint\frac{\mathrm{d}\omega_1}{2\pi}\frac{\mathrm{d}\omega_2}{2\pi} \hat{G}_{1i}(\varepsilon+\omega_1)\hat{Q}_{1j}\hat{G}_{ij}(\varepsilon+\omega_1+\omega_2)\hat{Q}_{i2}\hat{G}_{j2}(\varepsilon+\omega_2). \quad (117)$$

In the Feynman technique, as compared to the Goldstone technique, we avoid the need for a summation over the complete set of states, but instead require integration over frequencies. Note that $\Sigma = \Sigma_{\mathrm{d}} + \Sigma_{\mathrm{x}}$ is also called the self-energy operator. Comparison between Feynman and Goldstone shown in Table 9.

7.4 Feynman to Goldstone transformation

Here, we show the connection between the Feynman and Goldstone approaches, by demonstrating the Feynman expressions reduce to the Goldstone ones by integration over frequencies.

Inserting (114) into the direct term (116), we get

$$\Sigma^{(2)}_{\mathrm{d}} = i\iint \mathrm{d}^3r_i\mathrm{d}^3r_j\int\frac{\mathrm{d}\omega}{2\pi}\hat{G}_{12}(\varepsilon+\omega)\hat{Q}_{1i}\hat{Q}_{j2} \times\sum_a\left(|a\rangle_2\langle a|_1\hat{G}^{\mathrm{ex}}_{12}(\varepsilon_a-\omega)+|a\rangle_1\langle a|_2\hat{G}^{\mathrm{ex}}_{21}(\varepsilon_a+\omega)\right). \quad (118)$$

The two required frequency integrals:

$$\int\frac{\mathrm{d}\omega}{2\pi}\hat{G}_{12}(\varepsilon+\omega)\hat{G}^{\mathrm{ex}}_{ij}(\varepsilon_a-\omega) = -i\sum_{nm}\frac{|n\rangle_1\langle n|_2\,|m\rangle_i\langle m|_j}{\varepsilon+\varepsilon_a-\varepsilon_m-\varepsilon_n},$$
$$\int\frac{\mathrm{d}\omega}{2\pi}\hat{G}_{12}(\varepsilon+\omega)\hat{G}^{\mathrm{ex}}_{ji}(\varepsilon_a+\omega) = -i\sum_{bn}\frac{|b\rangle_1\langle b|_2\,|n\rangle_j\langle n|_i}{\varepsilon-\varepsilon_a-\varepsilon_b+\varepsilon_n}, \quad (119)$$

are evaluated using Eqs. (111) and (110), respectively, noting that only the excited states appear in the expansion for G^{ex}. Bringing these together, and evaluating the direct matrix element (using notation $|ab\rangle_{12} = |a\rangle_1|b\rangle_2$), we have:

$$\begin{aligned}\delta\varepsilon^{\mathrm{d}}_v &= \langle v|\Sigma^{(2)}_{\mathrm{d}}|v\rangle \\ &= \sum_{anm}\frac{\langle va|Q|nm\rangle\langle mn|Q|av\rangle}{\varepsilon+\varepsilon_a-\varepsilon_m-\varepsilon_n} + \sum_{abn}\frac{\langle vn|Q|ba\rangle\langle ab|Q|nv\rangle}{\varepsilon-\varepsilon_a-\varepsilon_b+\varepsilon_n} \\ &= \sum_{anm}\frac{g_{vanm}g_{mnav}}{\varepsilon+\varepsilon_a-\varepsilon_m-\varepsilon_n} + \sum_{abn}\frac{g_{vnba}g_{abnv}}{\varepsilon-\varepsilon_a-\varepsilon_b+\varepsilon_n}, \end{aligned} \quad (120)$$

which is the expression from Goldstone diagrams (a) and (c).

Table 9: Expectation values of the direct part of the correlation potential $\langle v|\Sigma_d|v\rangle$ for the lowest valence states of Cs (atomic units). The first four rows correspond to the second-order Goldstone technique using various number of states in the MBPT expansion, and the fifth row is the second-order Feynman technique. The final two rows are the screening and hole-particle corrections (see below).

	$6s_{1/2}$	$6p_{1/2}$	$6p_{3/2}$	$5d_{3/2}$	$5d_{5/2}$
30spdfghi	-0.01906	-0.00771	-0.00693	-0.01226	-0.01182
40spdfghi	-0.01915	-0.00768	-0.00690	-0.01228	-0.01182
50spdfghi	-0.01919	-0.00769	-0.00691	-0.01230	-0.01184
60spdfghi	-0.01920	-0.00769	-0.00691	-0.01230	-0.01184
Feynman	-0.01920	-0.00766	-0.00689	-0.01236	-0.01190
δScreen	0.00631	0.00246	0.00221	0.00331	0.00313
δh-p	-0.00769	-0.00359	-0.00322	-0.00477	-0.00457

For the exchange term, we first integrate over ω_1, with:

$$\begin{aligned}
&\int \frac{\mathrm{d}\omega_1}{2\pi}\hat{G}_{1i}(\varepsilon+\omega_1)\hat{G}_{ij}(\varepsilon+\omega_1+\omega_2)\\
=&i\sum_{an}\left(\frac{|a\rangle_1\langle a|_i|n\rangle_i\langle n|_j}{\omega_2+\varepsilon_a-\varepsilon_n}+\frac{|n\rangle_1\langle n|_i|a\rangle_i\langle a|_j}{-\omega_2+\varepsilon_a-\varepsilon_n}\right)\\
=&i\sum_{a}\left[|a\rangle_1\langle a|_i\,\hat{G}^{\mathrm{ex}}_{ij}(\varepsilon_a+\omega_2)+\hat{G}^{\mathrm{ex}}_{1i}(\varepsilon_a-\omega_2)\,|a\rangle_i\langle a|_j\right] \qquad (121)\\
\equiv&i\,\hat{\Gamma}_{1iij}(\omega_2) \qquad (122)
\end{aligned}$$

which was evaluated using Eq. (110). The Γ_{1iij} term is defined for notational brevity; note the similarity+difference to Π_{ij}. This leads to two seperate integrals over ω_2:

$$\begin{aligned}
\int \frac{\mathrm{d}\omega_2}{2\pi}\hat{G}^{\mathrm{ex}}_{ij}(\varepsilon_a+\omega_2)\hat{G}_{j2}(\varepsilon+\omega_2) &= i\sum_{bn}\frac{|n\rangle_i\langle n|_j|b\rangle_j\langle b|_2}{\varepsilon_a-\varepsilon+\varepsilon_b-\varepsilon_n},\\
\int \frac{\mathrm{d}\omega_2}{2\pi}\hat{G}^{\mathrm{ex}}_{1i}(\varepsilon_a-\omega_2)\hat{G}_{j2}(\varepsilon+\omega_2) &= i\sum_{nm}\frac{|m\rangle_1\langle m|_i|n\rangle_j\langle n|_2}{\varepsilon_m+\varepsilon_n-\varepsilon-\varepsilon_a},
\end{aligned} \qquad (123)$$

which were evaluated using Eqs. (110) and (111), respectively. Finally, combining all the terms, we have:

$$\begin{aligned}
\delta\varepsilon^{\mathrm{x}}_v &= \langle v|\Sigma^{(2)}_{\mathrm{x}}|v\rangle\\
&= -\sum_{abn}\frac{\langle vn|Q|ab\rangle\langle ab|Q|vn\rangle}{\varepsilon-\varepsilon_a-\varepsilon_b+\varepsilon_n}-\sum_{anm}\frac{\langle va|Q|mn\rangle\langle mn|Q|av\rangle}{\varepsilon+\varepsilon_a-\varepsilon_m-\varepsilon_n}\\
&= -\sum_{anm}\frac{g_{vnab}g_{abvn}}{\varepsilon-\varepsilon_a-\varepsilon_b+\varepsilon_n}-\sum_{abn}\frac{g_{vman}g_{mnav}}{\varepsilon+\varepsilon_a-\varepsilon_m-\varepsilon_n}, \qquad (124)
\end{aligned}$$

which is exactly the expression from Goldstone diagrams (d) and (b), respectively (note that $g_{ijkl}=g_{jilk}$).

7.5 Angular separation

Using the same angular identities used for the Goldstone case:

$$\sum_{m_{i,j,k,l}} g_{ijkl}\,g_{lkji} = \sum_{\mu}\frac{1}{[\mu]}\left(C^{\mu}_{ik}C^{\mu}_{jl}R^{\mu}_{ijkl}\right)^2 \qquad (125)$$

$$\begin{aligned}
\sum_{m_{i,j,k,l}} g_{ijkl}\,g_{klji} &= \sum_{\mu\lambda}(-1)^{\mu+\lambda+1}C^{\mu}_{ik}C^{\mu}_{jl}C^{\lambda}_{il}C^{\lambda}_{jk}\\
&\quad\times\begin{Bmatrix} j_i & j_k & \mu\\ j_j & j_l & \lambda\end{Bmatrix}R^{\mu}_{ijkl}R^{\lambda}_{ijlk} \qquad (126)\\
&= -\sum_{\mu\lambda}(-1)^{\mu+\lambda}L^{\mu\lambda}_{ijkl}\,R^{\mu}_{ijkl}R^{\lambda}_{ijlk}, \qquad (127)
\end{aligned}$$

where $L^{k\lambda}_{ijkl}$ is defined for convenience in the last line, the correlation potential (for angular state κ_v) can be written:

$$\Sigma^{(\kappa_v)}_{12,\mathrm{d}} = \int\frac{\mathrm{d}\omega}{2\pi}\sum_k\sum_{\alpha}^{(\kappa)}\frac{(C^k_{v\alpha})^2}{[j_v]}g^{\alpha}_{12}(\varepsilon+\omega)\sum_{ij}\hat{q}^k_{1i}\,\hat{\pi}^k_{ij}(\omega)\,\hat{q}^k_{j2}, \qquad (128)$$

$$\begin{aligned}
\Sigma^{(\kappa_v)}_{12,\mathrm{x}} &= \iint\frac{\mathrm{d}\omega_1}{2\pi}\frac{\mathrm{d}\omega_2}{2\pi}\sum_{k\lambda}\frac{(-1)^{k+\lambda}}{[j_v]}\sum_{\alpha,\beta,\gamma}^{(\kappa)}L^{k\lambda}_{v\beta\alpha\gamma}\\
&\quad\times\sum_{ij}g^{\alpha}_{1i}(\varepsilon+\omega_1)\,\hat{q}^k_{1j}\,g^{\beta}_{ij}(\varepsilon+\omega_1+\omega_2)\,\hat{q}^{\lambda}_{i2}\,g^{\gamma}_{j2}(\varepsilon+\omega_2). \qquad (129)
\end{aligned}$$

Here, the k sum is over Coulomb multipolarities, and the $(\kappa=\alpha,\beta,\gamma)$ sum is over angular quantum numbers (partial waves). In theory, the k and κ sums are infinite; in practice one (or both) must be truncated. The ij sum is the finite-grid implementation of radial integrals; the integration measures are included in q_{ij}. This means Σ is a coordinate matrix, and integration (even over external coordinates) is done implicitly in the matrix multiplication. The superscripts on the Σ operators denote that they are radial operators (the angular integrals have already been done):

$$\langle v|\hat{\Sigma}|v\rangle = \sum_{12}F^{\dagger}_v(r_1)\Sigma^{(\kappa_v)}_{12}F_v(r_2),$$

where $F(r)=(f,g)^{\mathrm{Tr}}$ is the radial spinor (see previous).

The radial Green's function is

$$g^{\alpha}_{12}(\varepsilon) = \sum_n^{\kappa_\alpha}\frac{F_{n\alpha}(r_1)F^{\dagger}_{n\alpha}(r_2)}{\varepsilon-\varepsilon_{n\alpha}} = \frac{\chi^{\alpha}_0(r_<)\chi^{\alpha}_{\infty}(r_>)}{w}, \qquad (130)$$

where the sum runs over all states with $\kappa=\kappa_\alpha$, and the χ are solutions to the radial Dirac equation with $\kappa=\kappa_\alpha$. As described above, g should be corrected to account for exchange, with

$$V^{(\kappa_v)}_{\mathrm{x},12} = \frac{-1}{[j_v]}\sum_a^{\mathrm{core}}\sum_{\lambda}(C^{\lambda}_{av})^2F_a(r_1)F^{\dagger}_a(r_2)\hat{q}^{\lambda}_{12}. \qquad (131)$$

The radial Coulomb operator is (see Laplace expansion)

$$\hat{q}^k_{ij} = \frac{r^k_<}{r^{k+1}_>}\,\mathrm{d}r_i\mathrm{d}r_j, \qquad (132)$$

and the radial polarisation operator is

$$\pi^k_{12}(\omega) = i\sum_a^{\mathrm{core}}p^a_{12}\sum_n^{(\kappa)}\frac{(C^k_{an})^2}{[k]}\left[g^{\mathrm{ex},n}_{12}(\varepsilon_a-\omega)+g^{\mathrm{ex},n}_{12}(\varepsilon_a+\omega)\right], \qquad (133)$$

where

$$p^a_{ij} = F_a(r_i)F^{\dagger}_a(r_j)$$

is the (radial) projection operator onto single core state a. and $g^{\mathrm{ex},n}$ contains only excited states with $\kappa=\kappa_n$.

7.6 Numerical frequency integration

The direct and exchange potentials involve integrals of the form:

$$\int g(\varepsilon+w)\pi(\omega)\ldots\frac{\mathrm{d}\omega}{2\pi}. \qquad (134)$$

The integrand contains poles from the Green's function at $\omega=\varepsilon_n-\varepsilon-i\delta$ and $\omega=\varepsilon_a-\varepsilon+i\delta$, and poles from the polarisation

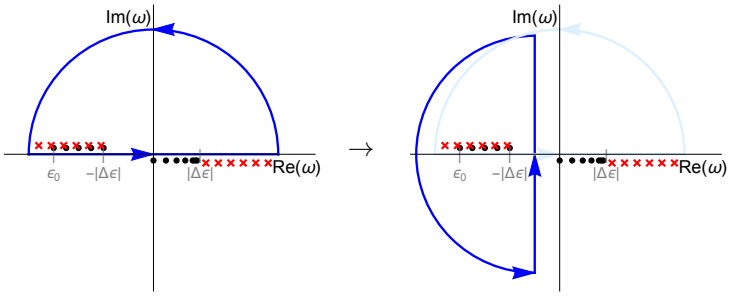

Figure 8: Rotation of the contour for integrals in the form of Eq. (134). Dots represent Green's function poles, crosses are polarisation operator poles (only bound-state poles are shown, there are also continuum-state poles at larger $|\omega|$), ε_0 is the energy of the deepest core state, and $|\Delta\varepsilon|$ is the energy gap between the core and excited bound states.

operator at $\omega = \varepsilon_a - \varepsilon_n + i\delta$ and $\omega = \varepsilon_n - \varepsilon_a - i\delta$. If ε is the energy of the lowest excited state, then there are an infinite number of poles from the polarisation operator in each of the regions $\omega < -|\Delta\varepsilon|$, and $|\Delta\varepsilon| < \omega < \infty$, where $\Delta\varepsilon$ is the energy gap between the highest core and lowest excited states (for Cs, $|\Delta\varepsilon| \approx 0.7\,\text{au}$). From the Green's function, there are a finite number (equal to the number of core states) of poles in the region $-|\varepsilon_0| < \omega < -|\Delta\varepsilon|$, and an infinite number of poles in the region $\omega > 0$ (see Fig. 8).

In theory, we could evaluate the integral (134) numerically using a semi-circle contour closed in the upper/lower-half of the complex plain, as done previously. However, this would involve evaluating the integrand very (arbitrarily) close to the poles, which is problematic. Instead, we rotate the integration contour anti-clockwise by 90°; the straight part of the contour is at fixed $\text{Re}(\omega)$. This is shown in Fig. 8. It is clear from Cauchy's theorem that the integral over each of the contours is the same and equal to the required integral (134).

Using the contour as shown in Fig. 8, the integral becomes

$$\int_{-\infty}^{\infty} g(\varepsilon+\omega_r+i\omega_i)\pi(\omega_r+i\omega_i)\ldots\frac{\mathrm{d}\omega_i}{2\pi} + \int_{\text{curved}}^{0}\ldots. \qquad (135)$$

If the contour radius (i.e., maximum value of ω_i) is large enough, the value of the integrand around the curved part of the contour ≈ 0, so only the ω_i integral needs to be evaluated. It is desirable to place ω_r, which remains constant throughout the integration, as far away from the poles as possible. There is a region with no poles between 0 and $|\Delta\varepsilon|$, so we take $\omega_r \simeq -|\Delta\varepsilon|/2$.

Finally, to perform the integrals numerically, we must evaluate Green's functions at complex values of $\omega = \omega_r + i\omega_i$. This can be done in analogy with Eq. (104):

$$g(\varepsilon+\omega) = \left[1 + i\omega_i g(\varepsilon+\omega_r)\right]^{-1} g(\varepsilon+\omega_r) \qquad (136)$$

This $g(\varepsilon+\omega)$ will be a complex-valued matrix; $g(\varepsilon+\omega_r)$ is real-valued. The integration over ω_i can proceed using standard numerical integration.

8 All-orders correlation potential

The three most important corrections beyond the second-order correlation potential are: (i) the screening of the residual Coulomb interaction by the core electrons [25], (ii) the hole-particle interaction [27], and (iii) the chaining of the Σ operator [20, 21]. These effects are described by a series of diagrams

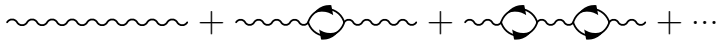

Figure 9: Screening of the Coulomb interaction: each Coulomb line is replaced with this infinite series of screening diagrams.

that can be summed exactly to all-orders using the Feynman technique. The method described here was developed in the above works, and can be called the *Dzuba-Flambaum-Sushkov* (DFS) method; it is sometimes also called the *correlation potential in the screened Coulomb interaction* (CPSCI) method.

It is important to stress a key advantage of the current method: its numerical efficiency. Using the Feynman approach for the second-order (direct) diagrams takes roughly the same computational power as using the Goldstone method (in fact, it is a bit faster). Then, the inclusion of the all-orders screening and hole-particle interaction has effectively *no* impact on the computer time required. That is, calculating the all-orders correlation potential is roughly just as computationally intensive as calculating the second-order corrections using the usual (Goldstone) many-body approach. This is in stark contrast to other methods (e.g., coupled-cluster methods), which require *huge* computational resources for all-orders calculations.

8.1 Screening of the residual Coulomb interaction

The most important correction is the the screening of the residual Coulomb interaction by the core electrons, which can be taken into account by a continued insertion of polarisation loops into the Coulomb lines, as shown in Fig. 9. This chain of diagrams represent the matrix geometric series:

$$\widetilde{Q} \equiv \hat{Q} + \hat{Q}\hat{\Pi}\hat{Q} + \hat{Q}\hat{\Pi}\hat{Q}\hat{\Pi}\hat{Q} + \ldots, \qquad (137)$$

which may be summed exactly as

$$\widetilde{Q}(\omega) = \hat{Q}\left[1 - \hat{\Pi}(\omega)\hat{Q}\right]^{-1} = \left[1 - \hat{Q}\hat{\Pi}(\omega)\right]^{-1}\hat{Q}. \qquad (138)$$

This is called the screened Coulomb operator. The screening is enhanced by the number of electrons in the outermost core shell, and the relatively small energy denominator associated with their excitation, see Eq. (114). We could also instead write the series (137) as $Q\widetilde{\Pi}Q$, with

$$\widetilde{\Pi}(\omega) = \hat{\Pi}(\omega)\left[1 - \hat{Q}\hat{\Pi}(\omega)\right]^{-1} = \left[1 - \hat{\Pi}(\omega)\hat{Q}\right]^{-1}\hat{\Pi}(\omega). \qquad (139)$$

Inserting the screened Coulomb operator into Eqs. (116) and (117) yields the new correlation potential:

$$\Sigma_{\text{d}} = \iint \mathrm{d}^3r_i d^3r_j \int \frac{\mathrm{d}\omega}{2\pi}\hat{G}_{12}(\varepsilon+\omega)\hat{Q}_{1i}\hat{\Pi}_{ij}(\omega)\widetilde{Q}_{j2}(\omega), \qquad (140)$$

$$\Sigma_{\text{x}} = -\iint \mathrm{d}^3r_i d^3r_j \iint \frac{\mathrm{d}\omega_1}{2\pi}\frac{\mathrm{d}\omega_2}{2\pi}\times \hat{G}_{1i}(\varepsilon+\omega_1)\widetilde{Q}_{1j}(\omega_1)\hat{G}_{ij}(\varepsilon+\omega_1+\omega_2)\widetilde{Q}_{i2}(\omega_2)\hat{G}_{j2}(\varepsilon+\omega_2), \qquad (141)$$

which includes screening to all-orders. Note that the screened operator should replace only a single Coulomb line in the direct diagram, but both in the exchange diagram.

Note that this method takes into account screening diagrams with double, triple, quadruple, and higher core electron excitations. This is because the Feynman diagram technique contains all possible time orderings of the polarisation loops; therefore the screening diagrams contain any number of excited electrons [25]. This is in contrast to the widely-used "singles-doubles

Figure 10: Hole-particle corrections to the polarisation operator

coupled-cluster method", where only double excitations are considered (and sometimes a selection of important triple excitations). There are, however, some perturbation-theory diagrams included in the coupled-cluster methods that are not included in our approach. The most important of which, the so-called ladder diagrams, are very small, and can be included into our method by means of the method presented in Ref. [29].

8.2 Hole-particle interaction

The chain of diagrams corresponding to the hole-particle interaction is shown in Fig. 10. Physically, this effect arises due to the deviation of the (direct) Hartree-Fock potential for the excited core electron in the polarisation loop from that for the non-excited one [27]. In other words, it corresponds to an alteration of the core potential due to the excitation of the particle from the core to the virtual intermediate state; the excited core particle in the polarisation loop moves in the field of $N-2$ other core electrons instead of the usual V^{N-1} potential.

In practical Hartree-Fock calculations for occupied core states, the self-interaction term is included in the direct potential; this is then exactly compensated by the corresponding term in the exchange potential. However, for the state excited from the core ($a_n^\dagger a_a|0\rangle$), no such cancellation occurs. Therefore, the self-interaction term should be removed for the excited states.

Following the approach from Ref. [27], the potential that simultaneously describes the occupied core and excited states is

$$\hat{V} = V^{N-1} - (1-\hat{P}_{\rm core})V_0(1-\hat{P}_{\rm core}), \tag{142}$$

where

$$\hat{P}_{\rm core} = \sum_a^{\rm core} |a\rangle\langle a| \tag{143}$$

is the operator of projection onto the core, and V_0 is the zero-multipolarity potential for the "outgoing electron". We use Eq. (142) since the calculated Green's function contains both core and excited electrons [see Eq. (100)]; $\hat{P}$ is introduced to ensure orthogonality of the orbitals. The excited-states Green's function that appears in the polarisation operator is then formed as Eq. (115). Note that $\langle V\rangle = \langle V^{N-1}\rangle$ for the occupied core states, and $\langle V\rangle = \langle V^{N-1}\rangle - \langle V_0\rangle$ for the excited states. In this method, we do not calculate the hole-particle diagrams directly. We calculate the Green's function using the potential in Eq. (142), and use it to form the polarisation operator. This corrected polarisation operator includes the dominating hole-particle effects.

We may include the "corrected" polarisation operator in place of the regular polarisation operator when calculating the screened Coulomb line, as shown in Fig. 11. Inserting the corrected polarisation loop, and the screened Coulomb lines into the diagrams for the correlation potential, we obtain an expression for the all-order correlation potential as shown in Fig. 12.

8.3 Self-energy chaining

The "chaining" of the correlation potential (iteration of Σ) is shown in Fig. 13. This is accounted for automatically by including Σ into the Hartree-Fock iterations for the valence orbital (correlation potential method, as described previously).

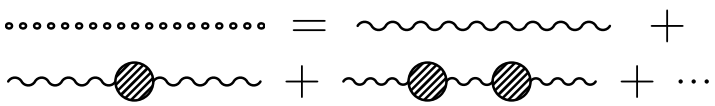

Figure 11: All-order screening of the Coulomb operator including the hole-particle interaction.

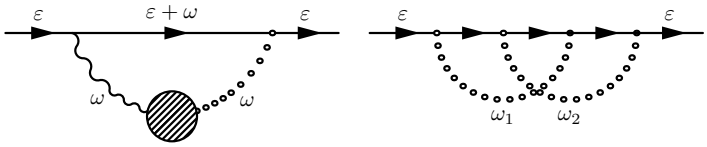

Figure 12: All-order correlation diagrams including the Coulomb screening and hole-particle interaction.

This is an important effect that includes terms with excitations of the external valence electron, and is enhanced due to the small energy denominator associated with this excitation. Because the Hartree-Fock equations (with Σ) are iterated until self-consistancy is reached, the chaining is included to all-orders.

8.4 Effective screening for exchange term

In the all-orders method, the frequency integrations can no longer be performed analytically. This is fine for the direct potential, since it contains only a single integral (the frequency integral inside the polarisation operator can be done analytically). The exchange potential, on the other hand, contains a double integral over frequencies, which is numerically expensive.

The exchange contribution to the correlation potential is typically small compared to the direct potential, and the screening is a small correction to this. Therefore, it seems reasonable to approximately account for the screening in the exchange potential. This is done by introducing effective screening factors for the Coulomb operator in the exchange potential: $\tilde{Q} \approx f\hat{Q}$. In practice, the Coulomb operator is expanded over multipolarities $\hat{Q} \sim \sum_k \hat{q}^k$ (Laplace expansion, as discussed previously), and a different screening factor is used for each multipolarity:

$$\tilde{q}^k(\omega) \approx f_k \hat{q}^k. \tag{144}$$

Note that the frequency dependence of f_k has been neglected.

The screening factors are calculated by evaluating the direct energy correction (for each k) with and without screening:

$$f_k = \langle v|\Sigma_{\rm d}^{({\rm screened}),k}|v\rangle \,/\, \langle v|\Sigma_{\rm d}^{(2),k}|v\rangle. \tag{145}$$

Then, the frequency integrals for the exchange term can be carried out analytically, and the exchange potential may be calculated by summation over a complete set of states in exact analogy to the Goldstone case, just with the extra k-dependent factors. This greatly improves the efficiency of the exchange part of the calculation, while still maintaining good accuracy.

The hole-particle interaction is not included in Σ for calculation of f_k (hole-particle effect enters at third-order in the direct diagrams, but only at fourth-order in exchange). However, this means the hole-particle effect is not included into the exchange diagrams at all, which in certain cases may be important. The screening effect is also taken into account approximately, which may also be important in some cases.

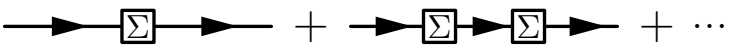

Figure 13: Chaining of the correlation potential (self-energy); the boxed Σ refers to the sum of diagrams in Fig. 12.

9 Relativity beyond Dirac-Coulomb (Breit+QED)

The Dirac equation as presented in Eq. (24) accounts for the relativistic motion of the electron in the Coulomb field of the nucleus, however, it treats the Coulomb field classically, and treats the electron-electron Coulomb repulsion non-relativistically (see, e.g., Ref. [1]). For high-accuracy calculations, and particularly for atoms with large Z, corrections due to the missing relativistic effects become important ($\sim 0.1-1\%$). The two corrections considered here are the Breit interaction, which contains the dominating relativistic corrections to the electron-electron Coulomb interaction, and the radiative quantum electrodynamics (QED) corrections, which are accounted for via the Ginges-Flambaum radiative potential method.

9.1 Breit interaction[23]

This section mostly follows Ref. [3]; see also [30–32]. The Breit Hamiltonian accounts for magnetic interactions between electrons (known as the Gaunt interaction), and retardation effects (see, e.g., [1]). It leads to a correction to the electron-electron Coulomb term in the many-body Hamiltonian (24):

$$\sum_{ij}\frac{1}{r_{ij}} \to \sum_{ij}\left(\frac{1}{r_{ij}}+\hat{h}^B_{ij}\right), \tag{146}$$

where, in the limit of zero frequency, the two-particle Breit Hamiltonian is

$$\hat{h}^B_{ij} = -\frac{\boldsymbol{\alpha}_i\cdot\boldsymbol{\alpha}_j + (\boldsymbol{\alpha}_i\cdot\hat{\boldsymbol{n}}_{ij})(\boldsymbol{\alpha}_j\cdot\hat{\boldsymbol{n}}_{ij})}{2\,\boldsymbol{r}_{ij}}. \tag{147}$$

Frequency-dependent effects can be neglected in most situations, see, e.g., discussion in Refs. [1, 3].

Inclusion of the Breit Hamiltonian into the Hartree-Fock equations [32] leads to a correction to the HF potential (27):

$$\hat{V}_{\rm HF} \to \hat{V}_{\rm HF} + \hat{V}_{\rm Br}. \tag{148}$$

Inclusion into the Hartree-Fock and TDHF equations allows for the inclusion of Breit effects into the calculations of atomic energies and wavefunctions. For the TDHF equations, an extra term now also appears:

$$\delta V \to \delta V_{\rm HF}(\delta\phi) + \delta V_{\rm Br}(\delta\phi), \tag{149}$$

which in fact gives the dominant Breit correction to matrix elements in many cases.

After integration over angular coordinates, and summation over magnetic quantum numbers, the (non-local) radial Breit operator can be expressed via

$$\hat{V}_{\rm Br}F_a(r) = \sum_b^{\rm core}\sum_k \hat{B}^k_{ba}F_b(r), \tag{150}$$

with

$$\hat{B}^k_{ba} = \frac{(C^k_{ba})^2}{[j_a]}\left[\hat{M}^k_{ba}+\hat{O}^k_{ba}+\hat{P}^k_{ba}\right] + \frac{(C^k_{-b,a})^2}{[j_a]}\hat{N}^k_{ba}. \tag{151}$$

[23] Implemented in: /src/HF/Breit.hpp

where M, N are due to the Gaunt effect, O, P are due to retardation, and $C^k_{-b,a} \equiv \langle -\kappa_b||C^k||\kappa_a\rangle$. The equation for $\delta V_{\rm Br}(\delta\phi)$ is not given explicitly here, but can be found by making the substitution in Eq. (72):

$$C^k_{ba}y^k_{ba} \to -C^k_{ba}(M^k_{ba}+O^k_{ba}+P^k_{ba}) - C^k_{-b,a}N^k_{ba}.$$

Note that while no direct Breit term appears in the HF equations, it does enter into $\delta V_{\rm Br}$.

The two Gaunt terms can be expressed as

$$\hat{M}^k_{ba} = \frac{k+1}{2k+3}\left[b^{k+1}_{ba}(r)+\eta^{k+1}_{ba}g^{k+1}_{ba}(r)\right]\left(\eta^{k+1}_{ba}\hat{\theta}_x-\hat{\theta}_y\right) - \frac{k}{2k-1}\left[b^{k-1}_{ba}(r)-\eta^{k}_{ba}g^{k-1}_{ba}(r)\right]\left(\eta^{k+1}_{ba}\hat{\theta}_x+\hat{\theta}_y\right) \tag{152}$$

and

$$\hat{N}^k_{ba}(r) = \frac{(\kappa_b+\kappa_a)^2}{k(k+1)}\,g^k_{ba}(r)\,\hat{\theta}_x, \tag{153}$$

and the two retardation terms can be expressed as

$$\hat{O}^k_{ba}(r) = \frac{(k+1)^2}{[k](2k+3)}\left[b^{k+1}_{ba}(r)+\eta^{k+1}_{ba}g^{k+1}_{ba}(r)\right]\left(-\eta^{k+1}_{ba}\hat{\theta}_x+\hat{\theta}_y\right) + \frac{k^2}{[k](2k-1)}\left[b^{k-1}_{ba}(r)-\eta^{k}_{ba}g^{k-1}_{ba}(r)\right]\left(\eta^{k+1}_{ba}\hat{\theta}_x+\hat{\theta}_y\right), \tag{154}$$

and

$$\hat{P}^k_{ba}(r) = \frac{k(k+1)}{2[k]}\Big[P_1(r)\left(\eta^{k+1}_{ba}\hat{\theta}_x-\hat{\theta}_y\right) - P_2(r)\left(\eta^{k}_{ba}\hat{\theta}_x+\hat{\theta}_y\right)\Big] \tag{155}$$

with

$$P_1(r) = \left[b^{k-1}_{0,ba}(r)-\eta^k_{ba}g^{k-1}_{0,ba}(r)-b^{k+1}_{0,ba}(r)+\eta^k_{ba}g^{k+1}_{0,ba}(r)\right]$$
$$P_2(r) = \left[b^{k-1}_{\infty,ba}(r)+\eta^{k+1}_{ba}g^{k-1}_{\infty,ba}(r)-b^{k+1}_{\infty,ba}(r)-\eta^{k+1}_{ba}g^{k+1}_{\infty,ba}(r)\right].$$

In the above,

$$\hat{\theta}_x = \begin{pmatrix}0 & 1\\ 1 & 0\end{pmatrix}, \quad \hat{\theta}_y = \begin{pmatrix}0 & 1\\ -1 & 0\end{pmatrix} \tag{156}$$

(note: $\hat{\theta}_x = \hat{\sigma}_x$, and $\hat{\theta}_y = i\hat{\sigma}_y$, except these act in the radial spinor space only), $\eta^k_{ba} \equiv (\kappa_b-\kappa_a)/k$,

$$b^k_{ij}(r) = \int_0^r \frac{x^k}{r^{k+1}}[f_ig_j-g_if_j](x)\,{\rm d}x + \int_r^\infty \frac{r^k}{x^{k+1}}[f_ig_j-g_if_j](x)\,{\rm d}x, \tag{157}$$

(with b_0/b_∞ being just the first/second term), and

$$g^k_{ij}(r) = \int_0^r \frac{x^k}{r^{k+1}}[f_ig_j+g_if_j](x)\,{\rm d}x + \int_r^\infty \frac{r^k}{x^{k+1}}[f_ig_j+g_if_j](x)\,{\rm d}x. \tag{158}$$

9.2 Radiative QED corrections[24]

Radiative QED corrections can be included into the wavefunctions using the radiative potential method developed in Ref. [33],

[24] Functions defined in: /src/Physics/RadiativePotential.hpp

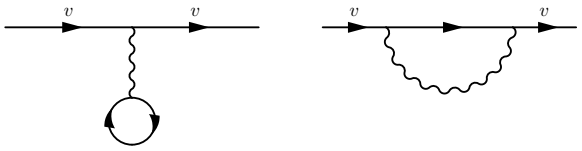

Figure 14: Vacuum polarisation (left) and self-energy (right) diagrams. In the radiative potential method, the self-energy diagram is replaced with an effective local potential [33].

including the (small) finite nuclear size corrections [34, 35]. In this method, an effective potential, $V_{\rm rad}$, is added to the Hamiltonian before the equations are solved. The potential can be written as the sum of the Uehling (vacuum polarisation) and self-energy potentials, see Fig. 14. The self-energy potential itself is written as the sum of the high- and low-frequency electric contributions, and the magnetic contribution:

$$V_{\rm rad}(\boldsymbol{r}) = V_{\rm Ueh}(r) + V^h_{\rm SE}(r) + V^l_{\rm SE}(r) + V^{\rm mag}_{\rm SE}(\boldsymbol{r}). \tag{159}$$

Including this potential into the Hartree-Fock equations (instead of adding it as a subsequent perturbation) gives an important contribution (core relaxation), especially for states with $l > 0$. The first three (electric) terms on the RHS of Eq. (159),

$$V^{\rm el}(r) = V_{\rm Ueh}(r) + V^h_{\rm SE}(r) + V^l_{\rm SE}(r), \tag{160}$$

are simple scalar terms, and can be included into the calculations simply (e.g., by adding them to the nuclear potential). The final (magnetic) term, which can be expressed as [35]

$$V^{\rm mag}_{\rm SE}(\boldsymbol{r}) = i(\boldsymbol{\gamma}\cdot\boldsymbol{n})H^{\rm mag}(r), \tag{161}$$

leads to off-diagonal terms in the Hamiltonian. Together, they can be included via additions to the radial derivative (12):

$$\partial_r F = \frac{1}{c}\begin{pmatrix} c(-\kappa/r + H^{\rm mag}) & (\varepsilon - \hat{V} + V^{\rm el} + 2c^2) \\ -(\varepsilon - \hat{V} + V^{\rm el}) & c(\kappa/r - H^{\rm mag}) \end{pmatrix} F. \tag{162}$$

The sign convention here for $V_{\rm rad}$ (i.e., with $\hat{H} \to \hat{H} - V_{\rm rad}$) is from Ref. [33]; in the code I define $H^{\rm el} = -V^{\rm el}$.

Detailed expressions for the individual contributions to $V_{\rm rad}$ are given in Refs. [33–35] – they involve some rather nasty integrals that must be evaluated carefully.[25] Due to the presence of double integrals, the high-frequency term $V^{hf}_{\rm SE}$ is quite expensive to calculate. To speed this up, we calculate it only every $n \approx 5$ points along the grid and use cubic interpolation for the intermediate points.

Tables 10 and 11 show the QED and Breit corrections to the lowest s and p energies and E1 matrix elements, respectively. These are shown at the Hartree-Fock/RPA levels, and do not include correlation corrections. The interplay between the Breit/QED and correlation corrections turns out to be important [32, 34, 35], so for high-accuracy calculations, the Breit and QED effects must be included from the beginning.

[25] Note: there is a small typo in Eq. (14) of Ref. [35] ($V^{\rm step}_{\rm high}$); the $r \le r_N$ and $r > r_N$ terms should be swapped.

Table 10: Breit and QED corrections to the removal energies of the lowest s and p states of Cs at the Hartree-Fock level (units: $\rm cm^{-1}$).

	HF	δBreit	δQED	Total
$6s_{1/2}$	−27954.06	3.20	15.97	−27934.93
$6p_{1/2}$	−18790.51	7.49	−0.80	−18783.82
$6p_{3/2}$	−18388.79	2.87	−0.11	−18386.03
$7s_{1/2}$	−12112.23	1.08	4.35	−12106.81
$7p_{1/2}$	−9222.63	2.69	−0.28	−9220.23
$7p_{3/2}$	−9079.24	1.05	−0.04	−9078.23

Table 11: Breit and QED corrections to the electrid dipole (E1) reduced matrix elements of lowest s and p states of Cs at the RPA level (units: $|e|a_B$).

	RPA	δBreit	δQED	Total
$6s_{1/2} - 6p_{1/2}$	−4.97441	0.00000	−0.00334	−4.97775
$6s_{1/2} - 7p_{1/2}$	−0.23873	−0.00161	0.00241	−0.23794
$6s_{1/2} - 6p_{3/2}$	7.01308	0.00013	0.00493	7.01814
$6s_{1/2} - 7p_{3/2}$	0.50874	0.00031	−0.00282	0.50624
$7s_{1/2} - 7p_{1/2}$	−10.92107	0.00113	−0.00687	−10.92680
$7s_{1/2} - 7p_{3/2}$	15.22745	0.00057	0.00985	15.23785
$6p_{1/2} - 7s_{1/2}$	4.44937	0.00454	−0.00444	4.44948
$6p_{3/2} - 7s_{1/2}$	6.71222	0.00185	−0.00557	6.70851

A Appendix

Some useful equations and definitions are given here; see also Refs. [2, 3, 5, 12, 36–38]. Note that notation differs between all these sources, I have introduced some notation not found in the above.

A.1 One- and two-body matrix elements for many-particle states

Let F and G be one- and two-particle operators

$$\hat{F} = \sum_i \hat{f}(\boldsymbol{r}_i) \quad , \qquad \hat{G} = \sum_{i<j} \hat{g}(\boldsymbol{r}_i, \boldsymbol{r}_j), \tag{A.1}$$

where $f(\boldsymbol{r}_i)$ acts on the ith electron; $g(\boldsymbol{r}_i, \boldsymbol{r}_j)$ acts on the pair of electrons $\{i, j\}$. Here, I use the short-hand notation from Ref. [2]:

$$|\Phi^n_i\rangle = a^\dagger_n a_i |\Phi\rangle,$$

with i, j denoting occupied states (core and valence), and m, n, denoting unoccupied virtual excited states. $|\Phi\rangle$ is a many-body Slater determinant wavefunction including the Hartree-Fock core and the occupied valence states (e.g., we may have $|\Phi\rangle = a^\dagger_v|0_{\rm HF}\rangle$), see Ref. [2]. Then, we have for diagonal matrix elements:

$$\begin{aligned} \langle\Phi|F|\Phi\rangle &= \sum_i \langle i|f|i\rangle = \sum_i f_{ii} \\ \langle\Phi|G|\Phi\rangle &= \sum_{i<j} \left(\langle ij|g|ij\rangle - \langle ji|g|ij\rangle\right) = \sum_{i<j} (g_{ijij} - g_{jiij}), \end{aligned} \tag{A.2}$$

for matrix elements between states that differ by a single orbital:

$$\begin{aligned} \langle\Phi^n_i|F|\Phi\rangle &= \langle n|f|i\rangle = f_{ni} \\ \langle\Phi^n_i|G|\Phi\rangle &= \sum_j \left(\langle nj|g|ij\rangle - \langle jn|g|ij\rangle\right) = \sum_j (g_{njij} - g_{jnij}), \end{aligned} \tag{A.3}$$

and for matrix elements between states that differ by two orbitals:

$$\begin{aligned} \langle\Phi^{nm}_{ij}|F|\Phi\rangle &= 0 \\ \langle\Phi^{nm}_{ij}|G|\Phi\rangle &= \langle nm|g|ij\rangle - \langle mn|g|ij\rangle = g_{nmij} - g_{mnij}. \end{aligned} \tag{A.4}$$

A.2 Coulomb Integrals[26]

The Coulomb integral g_{abcd} can be expressed:

$$g_{abcd} \equiv \int \mathrm{d}r_1^3 \mathrm{d}r_2^3\, \psi_a^\dagger(\boldsymbol{r_1})\psi_b^\dagger(\boldsymbol{r_2})\frac{1}{|\boldsymbol{r}_{12}|}\psi_c(\boldsymbol{r_1})\psi_d(\boldsymbol{r_2}) \tag{A.5}$$
$$= \sum_{kq}(-1)^q\langle\kappa_a m_a|C^k_{-q}|\kappa_c m_c\rangle\langle\kappa_b m_b|C^k_q|\kappa_d m_d\rangle R^k_{abcd},$$

where $\boldsymbol{r}_{12} = |\boldsymbol{r}_r - \boldsymbol{r}_2|$ is expanded over multipolarities, k:

$$\frac{1}{\boldsymbol{r}_{12}} = \sum_{kq}\frac{r^k_<}{r^{k+1}_>}(-1)^q C^k_{-q}(\boldsymbol{n}_1)C^k_q(\boldsymbol{n}_2), \tag{A.6}$$

with $r_< \equiv \min(r, r')$, and C^k_q is a spherical tensor:

$$C^k_q \equiv \sqrt{\frac{4\pi}{2k+1}}Y_{kq}(\boldsymbol{n}). \tag{A.7}$$

We also define the anti-symmetrised Coulomb integral [see (A.4)]:

$$\widetilde{g}_{abcd} = g_{abcd} - g_{abdc}. \tag{A.8}$$

It is easy to see that g is symmetric under $r_1 \leftrightarrow r_2$, and on interchange of initial/final states: $g_{abcd} = g_{badc} = g_{cdab} = g_{dcba}$.

The R^k_{abcd} factor (radial Coulomb integral) is defined:

$$R^k_{abcd} = \int \mathrm{d}r_1\ \left[f_a(r_1)f_c(r_1) + g_a(r_1)g_c(r_1)\right]\, y^k_{bd}(r_1), \tag{A.9}$$

which has symmetries: $c \leftrightarrow a,\ b \leftrightarrow d,\ (ac) \leftrightarrow (bd)$:

$$R^k_{abcd} = R^k_{cbad} = R^k_{adcb} = R^k_{cdab}$$
$$= R^k_{badc} = R^k_{bcda} = R^k_{dabc} = R^k_{dcba}, \tag{A.10}$$

and the symmetric $y^k_{bd}(r) = y^k_{db}(r)$ integral is defined:

$$y^k_{bd}(r) = \int_0^\infty \frac{r^k_<}{r^{k+1}_>}\left[f_a(r')f_b(r') + g_a(r')g_b(r')\right]\,\mathrm{d}r'. \tag{A.11}$$

The y^k_{bd} are often called Hartree screening functions.

The angular factor is defined:

$$C^k_{ab} \equiv \langle\kappa_a||C^k||\kappa_b\rangle \equiv (-1)^{j_a+1/2}\widetilde{C}^k_{ab}, \tag{A.12}$$
$$= (-1)^{j_a+1/2}\sqrt{[j_a][j_b]}\begin{pmatrix} j_a & j_b & k \\ -1/2 & 1/2 & 0\end{pmatrix}\pi(l_a+l_b+k), \tag{A.13}$$

where $\widetilde{C}^k_{ac}$ is a short-hand notation that is useful since $\widetilde{C}^k_{ac} = \widetilde{C}^k_{ca}$, and $\pi(x) = 1$ if x is even, but $= 0$ if x is odd.

We further define the useful integrals Q^k, W^k, and P^k:

$$Q^k_{abcd} \equiv (-1)^{k+j_a+j_b+1}\langle\kappa_a||C^k||\kappa_c\rangle\langle\kappa_b||C^k||\kappa_d\rangle R^k_{abcd}$$
$$= (-1)^k\widetilde{C}^k_{ac}\widetilde{C}^k_{bd}R^k_{abcd} \tag{A.14}$$
$$W^k_{abcd} \equiv Q^k_{abcd} + [k]\sum_\lambda\begin{Bmatrix} j_a & j_c & k \\ j_b & j_d & \lambda\end{Bmatrix}Q^\lambda_{abdc}$$
$$\equiv Q^k_{abcd} + P^k_{abcd}. \tag{A.15}$$

Q^k_{abcd} is convenient due to symmetries: $c \leftrightarrow a,\ b \leftrightarrow d,\ (ac) \leftrightarrow (bd)$.

Our Q^k and W^k is related to the X^k and Z^k from Ref. [2] as:

$$X^k_{abcd} \equiv (-1)^k\langle\kappa_a||C^k||\kappa_c\rangle\langle\kappa_b||C^k||\kappa_d\rangle R^k_{abcd}$$
$$= (-1)^{j_a+j_b+1}Q^k_{abcd} \tag{A.16}$$
$$Z^k_{abcd} = (-1)^{j_a+j_b+1}W^k_{abcd} \tag{A.17}$$

[26] Functions to calculate Coulomb integrals defined in: /src/Coulomb/, and functions for angular coefficients are in: /src/Angular/

Useful identities

See also the appendix of Ref. [12] for some very nice general angular identities (though note the minor notational difference between there and here; in particular, the Q^k terms differ by a factor of ±1. My definition is chosen here due to the symmetry properties).

$$\sum_{m_b} g_{abab} = [j_b]R^0_{abab}. \tag{A.18}$$

$$\sum_{m_{i,j,k,l}} g_{ijkl}\, g_{lkji} = \sum_\mu \frac{1}{[\mu]}\left(C^\mu_{ik}C^\mu_{jl}R^\mu_{ijkl}\right)^2 \tag{A.19}$$
$$= \sum_\mu \frac{1}{[\mu]}\left(Q^\mu_{ijkl}\right)^2 \tag{A.20}$$

$$\sum_{m_{i,j,k,l}} g_{ijkl}\, g_{klji} = \sum_{\mu\lambda}(-1)^{\mu+\lambda+1}C^\mu_{ik}C^\mu_{jl}C^\lambda_{il}C^\lambda_{jk}$$
$$\times\begin{Bmatrix} j_i & j_k & \mu \\ j_j & j_l & \lambda\end{Bmatrix}R^\mu_{ijkl}R^\lambda_{ijlk} \tag{A.21}$$
$$= -\sum_\mu \frac{1}{[\mu]}Q^\mu_{ijkl}P^\mu_{ijkl} \tag{A.22}$$

A.3 Angular integrals + identities

Wigner-Eckhardt theorem

$$\langle n_a\kappa_a m_a|T^k_q|n_b\kappa_b m_b\rangle$$
$$= (-1)^{j_a-m_a}\begin{pmatrix} j_a & k & j_b \\ -m_a & q & m_b\end{pmatrix}\langle n_a\kappa_a||T^k||n_b\kappa_b\rangle \tag{A.23}$$
$$\langle j||T^k||j'\rangle = (-1)^{j-j'}\langle j'||T^k||j\rangle^* \tag{A.24}$$

$$\langle J'IF'||T^k||JIF\rangle$$
$$= (-1)^{F+J'+I+k}\sqrt{[F'][F]}\begin{Bmatrix} J & I & F \\ F' & k & J'\end{Bmatrix}\langle J'||T^k||J\rangle \tag{A.25}$$

where $([a] \equiv 2a+1)$.

$$\sum_{m_a,m_b,q}|\langle n_a\kappa_a m_a|T^k_q|n_b\kappa_b m_b\rangle|^2 = |\langle n_a\kappa_a||T^k||n_b\kappa_b\rangle|^2. \tag{A.26}$$

Clebsch-Gordon coefficients notation

$$\langle j_1m_1, j_2m_2|JM\rangle \equiv (-1)^{j_1-j_2+M}\sqrt{[J]}\begin{pmatrix} j_1 & j_2 & J \\ m_1 & m_2 & -M\end{pmatrix} \tag{A.27}$$
$$\equiv C(j_1, j_2, J; m_1, m_2, M) \tag{A.28}$$
$$\equiv C^{JM}_{j_1m_1,j_2m_2}. \tag{A.29}$$
$$|j_1j_2; JM\rangle = \sum_{m_1,m_2}\langle j_1m_1, j_2m_2|JM\rangle|j_1m_1\rangle|j_2m_2\rangle \tag{A.30}$$

Some angular integrals + matrix elements

$$\sum_{jm}(2j+1)\begin{pmatrix} j_1 & j_2 & j \\ m_1 & m_2 & m\end{pmatrix}\begin{pmatrix} j_1 & j_2 & j \\ m'_1 & m'_2 & m\end{pmatrix} = \delta_{m_1m'_1}\delta_{m_2m'_2} \tag{A.31}$$

$$\sum_{m_1m_2}(2j+1)\begin{pmatrix} j_1 & j_2 & j \\ m_1 & m_2 & m\end{pmatrix}\begin{pmatrix} j_1 & j_2 & j' \\ m_1 & m_2 & m'\end{pmatrix} = \delta_{jj'}\delta_{mm'} \tag{A.32}$$

$$\int Y_{l'm'}Y_{lm}Y_{LM}\,\mathrm{d}\Omega$$
$$= \sqrt{\frac{[l'][l][L]}{4\pi}}\begin{pmatrix} l' & l & L \\ 0 & 0 & 0\end{pmatrix}\begin{pmatrix} l' & l & L \\ m' & m & M\end{pmatrix} \tag{A.33}$$

$$\sum_{m_l=-l}^{l} |Y_{lm_l}|^2 = \frac{2l+1}{4\pi} \quad , \qquad \sum_m |\Omega_{\kappa m}|^2 = \frac{2j+1}{4\pi} \tag{A.34}$$

$$\langle l_a||C^k||l_b\rangle = (-1)^{l_a}\sqrt{[l_a][l_b]}\begin{pmatrix} l_a & l_b & k \\ 0 & 0 & 0\end{pmatrix} \tag{A.35}$$

$$\langle n\kappa||r_z||n'\kappa'\rangle = (n\kappa|r|n'\kappa')\langle\kappa||C^1||\kappa'\rangle \tag{A.36}$$

From Ch. 13 of Ref. [38]:

$$\langle jls||l||j'l's'\rangle = \delta_{ll'}\delta_{ss'}(-1)^{j'+l+s+1}\sqrt{[j][j'][l]l(l+1)}\begin{Bmatrix} j & 1 & j' \\ l & s & l\end{Bmatrix} \tag{A.37}$$

$$\langle jls||s||j'l's'\rangle = \delta_{ll'}\delta_{ss'}(-1)^{j+l+s+1}\sqrt{[j][j'][s]s(s+1)}\begin{Bmatrix} j & 1 & j' \\ s & l & s\end{Bmatrix} \tag{A.38}$$

A.4 Useful definitions/identities

Dirac matrices

Dirac matrices are defined by the relation:

$$\{\gamma^\mu, \gamma^\nu\} = 2g^{\mu\nu}. \tag{A.39}$$

In the Dirac basis, they have the form:

$$\gamma^0 = \begin{pmatrix} 1 & 0 \\ 0 & -1\end{pmatrix}, \quad \gamma^a = \begin{pmatrix} 0 & \sigma^a \\ -\sigma^a & 0\end{pmatrix}, \quad \gamma^5 = \begin{pmatrix} 0 & 1 \\ 1 & 0\end{pmatrix}. \tag{A.40}$$

It is often convenient to also define: $\gamma^5 \equiv i\gamma^0\gamma^1\gamma^2\gamma^2$.

Pauli spin matrices

$$\sigma_x = \begin{pmatrix} 0 & 1 \\ 1 & 0\end{pmatrix}, \quad \sigma_y = \begin{pmatrix} 0 & -i \\ i & 0\end{pmatrix}, \quad \sigma_z = \begin{pmatrix} 1 & 0 \\ 0 & -1\end{pmatrix} \tag{A.41}$$

$$\sigma_i\sigma_j = i\epsilon_{ijk}\sigma_k + \delta_{ij}\,, \qquad [\sigma_i, \sigma_j] = 2i\epsilon_{ijk}\sigma_k \tag{A.42}$$

$$(\boldsymbol{\sigma}\cdot\boldsymbol{a})\,(\boldsymbol{\sigma}\cdot\boldsymbol{b}) = \boldsymbol{a}\cdot\boldsymbol{b} + i\boldsymbol{\sigma}\cdot(\boldsymbol{a}\times\boldsymbol{b}) \tag{A.43}$$

$$(\boldsymbol{\sigma}\cdot\boldsymbol{p})y(r)\Omega_{\kappa m} = i\left(y' + \frac{\kappa+1}{r}y\right)\Omega_{-\kappa,m} \tag{A.44}$$

$$(\boldsymbol{\sigma}\cdot\boldsymbol{n})\Omega_{\kappa m} = -\Omega_{-\kappa,m}, \tag{A.45}$$

Dirac orbitals (spherical potential, Dirac basis)

$$\phi_{n\kappa m}(\boldsymbol{r}) = \begin{pmatrix} f_{n\kappa}(r)\,\Omega_{\kappa m}(\boldsymbol{n}) \\ ig_{n\kappa}(r)\,\Omega_{-\kappa,m}(\boldsymbol{n})\end{pmatrix}, \tag{A.46}$$

$$\Omega_{\kappa m}(\boldsymbol{n}) = \sum_{\sigma=\pm1/2}\langle l, m-\sigma, 1/2, \sigma|j, m\rangle\, Y_{l,m-\sigma}(\boldsymbol{n})\,\chi_\sigma \tag{A.47}$$

$$= \begin{pmatrix} (-1)^{j-l-1/2}\sqrt{\frac{\kappa+1/2-m}{2\kappa+1}}Y_{l,m-1/2}(\theta,\phi) \\ \sqrt{\frac{\kappa+1/2+m}{2\kappa+1}}Y_{l,m+1/2}(\theta,\phi)\end{pmatrix} \tag{A.48}$$

(with $l \equiv |\kappa+1/2| - 1/2$), where

$$\kappa = (l-j)(2j+1)\,, \quad l = |\kappa+1/2| - 1/2\,, \quad j = |\kappa| - 1/2. \tag{A.49}$$

References

[1] H. A. Bethe and E. E. Salpeter, *Quantum mechanics of one-and two-electron atoms* (Plenum Publishing Corporation, New York, 1977).

[2] I. Lindgren and J. Morrison, *Atomic many-body theory*, 2nd ed. (Springer-Verlag, New York, 1986).

[3] W. R. Johnson, *Atomic Structure Theory* (Springer, New York, 2007).

[4] V. A. Dzuba, O. P. Sushkov, and V. V. Flambaum, Prepr. INP 82-89 **INP 82-89** (1982).

[5] J. Sapirstein, Rev. Mod. Phys. **70**, 55 (1998).

[6] G. B. Arfken, H. J. Weber, and F. E. Harris, *Mathematical Methods for Physicists* (Elsevier, 2013).

[7] A. E. S. Green, D. L. Sellin, and A. S. Zachor, Phys. Rev. **184**, 1 (1969).

[8] J. C. Slater, Phys. Rev. **81**, 385 (1951).

[9] W. R. Johnson, S. A. Blundell, and J. Sapirstein, Phys. Rev. A **37**, 307 (1988).

[10] K. Beloy and A. Derevianko, Comput. Phys. Commun. **179**, 310 (2008), arXiv:0710.3142.

[11] E. V. Kahl and J. C. Berengut, Comput. Phys. Commun. **238**, 232 (2019), arXiv:1805.11265.

[12] V. A. Dzuba, V. V. Flambaum, and O. P. Sushkov, J. Phys. B **17**, 1953 (1984).

[13] A. Dalgarno and J. T. Lewis, Proc. R. Soc. A **233**, 70 (1955).

[14] J. S. M. Ginges and V. V. Flambaum, Phys. Rep. **397**, 63 (2004).

[15] V. A. Dzuba, J. C. Berengut, J. S. M. Ginges, and V. V. Flambaum, Phys. Rev. A **98**, 043411 (2018), arXiv:1805.04989.

[16] N. L. Manakov, V. D. Ovsiannikov, and L. P. Rapoport, Phys. Rep. **141**, 320 (1986).

[17] W. R. Johnson, C. D. Lin, K. T. Cheng, and C. M. Lee, Phys. Scr. **21**, 409 (1980).

[18] W. R. Johnson, Adv. At. Mol. Opt. Phys. **25**, 375 (1989).

[19] A. Kramida, Y. Ralchenko, J. Reader, and The NIST ASD Team (2018), NIST At. Spectra Database (ver. 5.6.1) **[Online]**, http://physics.nist.gov/asd.

[20] V. A. Dzuba, V. V. Flambaum, P. G. Silvestrov, and O. P. Sushkov, Phys. Lett. A **103**, 265 (1984).

[21] V. A. Dzuba, V. V. Flambaum, P. G. Silvestrov, and O. P. Sushkov, J. Phys. B **18**, 597 (1985).

[22] G. Toh, A. Damitz, C. E. Tanner, W. R. Johnson, and D. S. Elliott, Phys. Rev. Lett. **123**, 073002 (2019), arXiv:1905.02768.

[23] M. S. Safronova, U. I. Safronova, and C. W. Clark, Phys. Rev. A **94**, 012505 (2016), arXiv:1605.05210.

[24] S. Pucher, P. Schneeweiss, A. Rauschenbeutel, and A. Dareau, Phys. Rev. A **101**, 042510 (2020), arXiv:1912.10089.

[25] V. A. Dzuba, V. V. Flambaum, P. G. Silvestrov, and O. P. Sushkov, Phys. Lett. A **131**, 461 (1988).

[26] A. A. Abrikosov, L. P. Gorkov, and I. E. Dzyaloshinski, *Methods of Quantum Field Theory in Statistical Physics* (Pergamon Press, 1965).

[27] V. A. Dzuba, V. V. Flambaum, and O. P. Sushkov, Phys. Lett. A **140**, 493 (1989).

[28] V. A. Dzuba, V. V. Flambaum, and J. S. M. Ginges, Phys. Rev. D **66**, 076013 (2002).

[29] V. A. Dzuba, Phys. Rev. A **78**, 042502 (2008).

[30] W. R. Johnson, S. A. Blundell, and J. Sapirstein, Phys. Rev. A **37**, 2764 (1988).

[31] J. B. Mann and W. R. Johnson, Phys. Rev. A **4**, 41 (1971).

[32] A. Derevianko, Phys. Rev. A **65**, 012106 (2001).

[33] V. V. Flambaum and J. S. M. Ginges, Phys. Rev. A **72**, 052115 (2005).

[34] J. S. M. Ginges and J. C. Berengut, J. Phys. B **49**, 095001 (2016).

[35] J. S. M. Ginges and J. C. Berengut, Phys. Rev. A **93**, 052509 (2016), arXiv:1603.09116.

[36] L. D. Landau and E. M. Lifshitz, *Quantum Mechanics: Non-relativistic Theory* (Pergamon, Oxford, 1977).

[37] I. I. Sobelman, *Atomic Spectra and Radiative Transitions* (Springer, Berlin, Heidelberg, 1992).

[38] D. A. Varshalovich, A. N. Moskalev, and V. K. Khersonskii, *Quantum Theory of Angular Momentum* (World Scientific, Singapore, 1988).